IMMUNOLOGY

Mitochondrial metabolic flexibility is critical for CD8$^+$ T cell antitumor immunity

Chao Chen[1], Hong Zheng[1], Edwin M. Horwitz[1], Satomi Ando[2]† , Koichi Araki[2]†, Peng Zhao[1], Zhiguo Li[1], Mandy L. Ford[3], Rafi Ahmed[2], Cheng-Kui Qu[1]*

Copyright © 2023 The Authors, some rights reserved; exclusive licensee American Association for the Advancement of Science. No claim to original U.S. Government Works. Distributed under a Creative Commons Attribution NonCommercial License 4.0 (CC BY-NC).

Mitochondria use different substrates for energy production and intermediatory metabolism according to the availability of nutrients and oxygen levels. The role of mitochondrial metabolic flexibility for CD8$^+$ T cell immune response is poorly understood. Here, we report that the deletion or pharmacological inhibition of protein tyrosine phosphatase, mitochondrial 1 (PTPMT1) significantly decreased CD8$^+$ effector T cell development and clonal expansion. In addition, *PTPMT1* deletion impaired stem-like CD8$^+$ T cell maintenance and accelerated CD8$^+$ T cell exhaustion/dysfunction, leading to aggravated tumor growth. Mechanistically, the loss of PTPMT1 critically altered mitochondrial fuel selection—the utilization of pyruvate, a major mitochondrial substrate derived from glucose—was inhibited, whereas fatty acid utilization was enhanced. Persistent mitochondrial substrate shift and metabolic inflexibility induced oxidative stress, DNA damage, and apoptosis in *PTPMT1* knockout cells. Collectively, this study reveals an important role of PTPMT1 in facilitating mitochondrial utilization of carbohydrates and that mitochondrial flexibility in energy source selection is critical for CD8$^+$ T cell antitumor immunity.

INTRODUCTION

Mitochondria produce energy [adenosine 5′-triphosphate (ATP)] and metabolites for macromolecule synthesis or as signaling molecules to regulate cell fate/function from the breakdown of carbohydrates, fats, and proteins. Mitochondrial abundance and their preferences for metabolic substrates differ in various cell types. While mitochondria in different types of cells or the same cell type in different functional states in the life cycle have distinct preferences for energy sources, they are flexible in using competing substrates for metabolism (*1*). Mitochondria switch freely between alternative substrates according to nutritional and physiological cues. Metabolically sensitive and flexible mitochondrial metabolic system in metabolic tissues is critically important for maintaining energy and metabolic homeostasis in response to physiological stress (starvation, exercise, etc.) and disease conditions (diabetes, metabolic disorders, etc.). However, it remains to be determined how mitochondrial utilization of various substrates is coordinated and how important mitochondrial robust and decisive shifts in substrate choice are for immune cells.

CD8$^+$ T cells play a central role in adaptive immunity against pathogens and tumor cells. During an immune response, upon cognate antigen stimulation and appropriate costimulatory signals, quiescent naïve CD8$^+$ T cells are activated, extensively proliferate, and differentiate into effector cells. Cytolytic CD8$^+$ effector T cells mediate primary adaptive immune responses against pathogens and tumor cells through proinflammatory cytokine secretion and direct killing of infected cells or tumor cells by the release of cytotoxic granules. Effector T cells can differentiate into memory T cells when the antigen is cleared. This long-lived memory CD8$^+$ T cell population remains quiescent and provides enhanced and rapid secondary immune responses when the same antigen is encountered. Effector T cells can also differentiate into a dysfunctional/exhausted state when antigen stimulation persists, but a small subset of exhausted T cells have stem cell–like characteristics, including self-renewal, persistence, and ability to differentiate into effector cells upon antigen restimulation (*2*–*6*). These stem-like CD8$^+$ T cells are the critical source for the proliferative burst and immune responses to checkpoint blockade therapy in cancer (*2*–*4*). Therefore, understanding the basic mechanisms of T cell exhaustion and stem-like CD8$^+$ T cell maintenance has important clinical implications.

There is considerable interest in understanding how metabolic programs coordinate the activities of CD8$^+$ T cells across different functional states and their role in antitumor immunity. CD8$^+$ T cell quiescence, activation, expansion, and function are regulated by complex cell-intrinsic mechanisms and microenvironmental signals. Emerging evidence indicates that cell metabolism is also a crucial regulator in shaping immune cell specification and function (*7*–*9*). Although previous studies on CD8$^+$ effector T cells identified a predominant role of aerobic glycolysis in boosting biosynthesis for rapid expansion (*10*, *11*), more recent evidence suggests that mitochondrial metabolism is also important for T cell immune responses (*12*–*15*). Despite the increasing investigation of mitochondrial functions in T cells, detailed mechanisms underlying mitochondrial regulation remain incomplete. Energy and biosynthesis demands in CD8$^+$ T cells change dynamically and rapidly in different functional states. Moreover, these immune cells experience constant changes in nutrients and oxygen levels in the circulation, various tissues, and at the sites where they perform functions such as the tumor microenvironment. It is poorly understood how their mitochondria

[1]Department of Pediatrics, Aflac Cancer and Blood Disorders Center, Winship Cancer Institute, Emory University School of Medicine, Atlanta, GA, 30322, USA. [2]Department of Microbiology and Immunology, Winship Cancer Institute, Emory University School of Medicine, Atlanta, GA, 30322, USA. [3]Department of Surgery, Winship Cancer Institute, Emory University School of Medicine, Atlanta, GA 30322, USA.
*Corresponding author. Email: cheng-kui.qu@emory.edu
†Present addresses: Division of Infectious Diseases, Center for Inflammation and Tolerance, Cincinnati Children's Hospital Medical Center, Cincinnati, OH 45229, USA; Department of Pediatrics, University of Cincinnati College of Medicine, Cincinnati, OH 45229, USA.

quickly switch metabolic substrates according to the availability of energy sources/oxygen and the energy/biosynthesis demands, and whether interruption of mitochondrial metabolic plasticity may affect $CD8^+$ T cell functions.

PTPMT1, a nuclear gene-encoded phosphatase, is localized to the mitochondrion and anchored at the inner membrane (*16*–*18*). Despite having a protein tyrosine phosphatase domain/motif, this phosphatase primarily dephosphorylates phosphatidylinositol phosphates (PIPs) (*17*, *18*), similar to the highly related phosphatase and tensin homolog (Pten) phosphatase. PTPMT1 is also involved in the synthesis of cardiolipin by converting phosphatidylglycerol phosphate to phosphatidylglycerol, the precursor of cardiolipin (*19*). Our previous studies have shown that PTPMT1 plays a critical role in the differentiation of embryonic stem cells (*18*) and

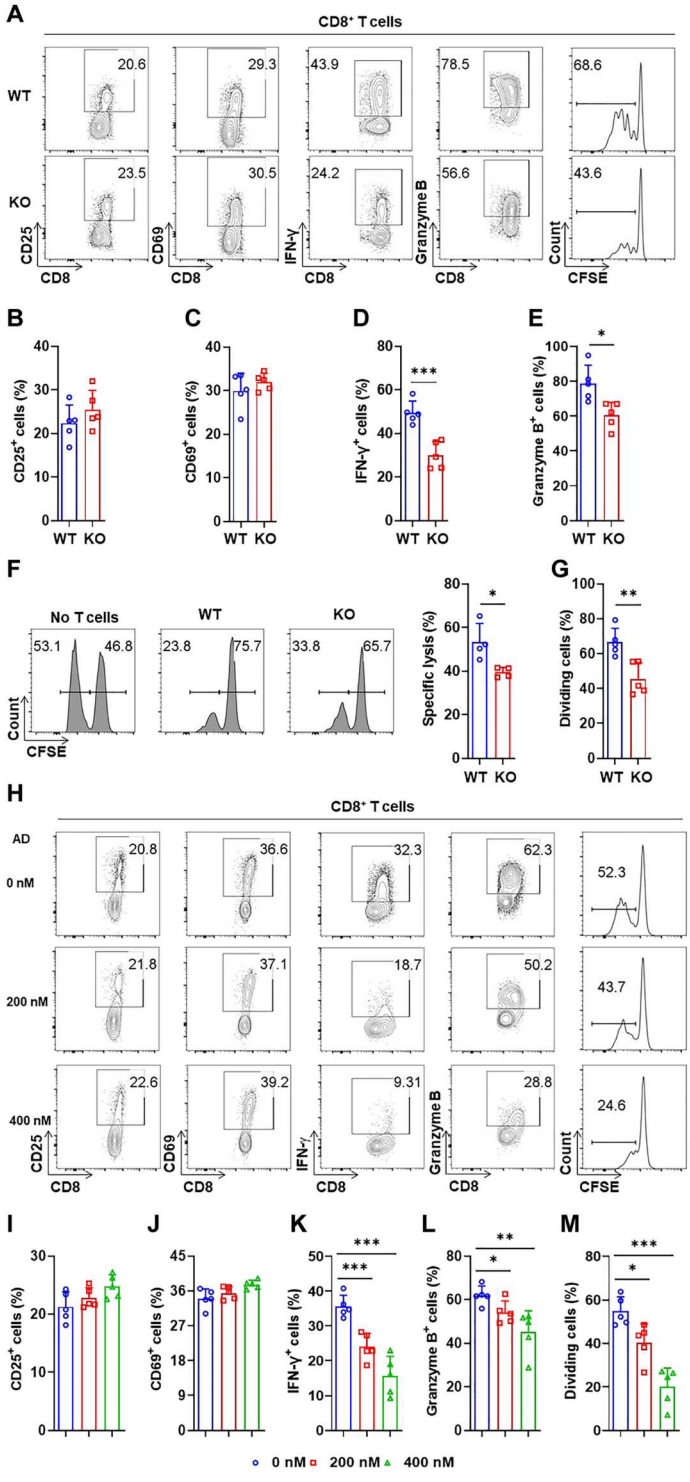

Fig. 1. Genetic deletion or pharmacological inhibition of PTPMT1 decreases $CD8^+$ effector cell development. (**A** to **F**) $CD8^+$ T cells isolated from *PTPMT1* KO and WT control mice were activated by CD3/CD28 antibody–coupled Dynabeads. The cells were analyzed by fluorescence-activated cell sorting (FACS) for the early activation markers CD25 and CD69 24 hours later [(A) to (C)]. Expression of IFN-γ and granzyme B was examined by FACS analyses at day 3 [(A), (D), and (E)]. (F) B16–ovalbumin (OVA) cells were used as target cells and stained in CFSE-low working solution (0.1 μM). Splenocytes were used as control cells and stained in CFSE-high working solution (1 μM). Cells were washed three times with phosphate-buffered saline (PBS). Target cells (CFSE-low) and control cells (CFSE-high) were mixed at the ratio of 1:1 and incubated with OVA peptide (SIINFEKL)–activated OT-I $CD8^+$ T cells for 4 to 5 hours. The cells were then analyzed by FACS. Specific lysis (%) = 100 − 100 × (% CFSE-low/% CFSE-high cells). (A) and (**G**) Cell division of CD3/CD28 antibody–activated $CD8^+$ T cells was determined by the CFSE dilution assay at day 3. (**H** to **M**) $CD8^+$ T cells isolated from WT C57BL/6 mice were activated in the presence of the PTPMT1 inhibitor AD at the indicated concentrations. The cells were examined for early activation markers CD25 and CD69, IFN-γ, granzyme B, and cell division as described above. Data are presented as means ± SD of biological replicates. *P < 0.05, **P < 0.01, and ***P < 0.001.

hematopoietic stem cells (*20*). The loss of *PTPMT1* blocks stem cells from producing progeny due to the activation of a bioenergetic stress–triggered cell cycle checkpoint and cell cycle arrest, while cell survival and self-renewal are not affected (*18*, *20*). PTPMT1 appears to function mainly by dephosphorylation of PIPs, which promote fatty acid–induced activation of mitochondrial uncoupling protein 2 (UCP2) (*18*, *20*), a C4 metabolite transporter (*21*), whose activation inhibits mitochondrial oxidation of glucose but enhances cytosolic glycolysis although the underlying mechanisms remain unclear (*22*–*25*). In the present study, we exploit a *PTPMT1* conditional knockout (KO) model to address PTPMT1-mediated metabolism in $CD8^+$ T cell immune responses. We find that PTPMT1 plays an important role in maintaining mitochondrial flexibility in fuel selection and that PTPMT1-facilitated mitochondrial oxidation of carbohydrates is essential for the development of effector T cells, the maintenance of stem-like $CD8^+$ T cells, and the prevention of $CD8^+$ T cell exhaustion.

RESULTS

PTPMT1 is required for optimal $CD8^+$ effector T cell development

To explore the role of PTPMT1-facilitated mitochondrial metabolism in T cells, we generated T cell–specific *PTPMT1* KO mice (*PTPMT1*$^{fl/fl}$/*Lck-Cre*$^+$). *PTPMT1* KO mice had normal thymocyte development, as demonstrated by comparable total thymocyte numbers (fig. S1A) and frequencies of thymocyte subpopulations (CD4/CD8–double negative, CD4/CD8–double positive, $CD4^+$, and $CD8^+$ cells) compared to wild-type (WT) *PTPMT1*$^{+/+}$/*Lck-Cre*$^+$ littermates (fig. S1, B to D). We also examined peripheral T cells in the spleen. Total splenocyte numbers (fig. S1A) and frequencies of T cell subpopulations ($CD4^+$, $CD8^+$, naïve, effector memory, and central memory T cells) in the spleen (fig. S1, E to H) were also similar between *PTPMT1* KO and WT control mice. These results suggest that PTPMT is dispensable for late thymocyte development or naïve peripheral T cell homeostasis (the Lck-Cre$^+$ transgene expresses the DNA recombinase Cre under the control of the Lck proximal promoter).

Analyses of the gene expression data in the BloodSpot database (*26*) showed that *PTPMT1* expression increased markedly in activated mouse $CD8^+$ and $CD4^+$ T cells (fig. S2A). *PTPMT1* expression was also up-regulated in activated human $CD8^+$ T cells based on the Monaco Scaled dataset in Human Protein Atlas (fig. S2B) (*27*), implying that PTPMT1 may play an important role in T cell functions. To test this possibility, we assessed the responses of *PTPMT1* KO $CD8^+$ T cells to the T cell receptor costimulations by anti-CD3 and anti-CD28 antibodies. We found that the initial activation of KO $CD8^+$ T cells was not affected according to the early activation markers CD25 and CD69 expressed on the cells (Fig. 1, A to C). However, effector cells derived from activated KO $CD8^+$ T cells were diminished as evidenced by significantly decreased interferon-γ (IFN-γ)–producing and granzyme B^+ cells in the resulting KO $CD8^+$ T cell population (Fig. 1, A, D, and E). Moreover, *PTPMT1*-deleted $CD8^+$ effector T cells were less effective in killing tumor cells in the cytotoxicity assay (Fig. 1F). The CFSE (carboxyfluorescein succinimidyl ester) dilution assay revealed that the cell division and cycling of *PTPMT1* KO cells were significantly reduced (Fig. 1, A and G). These data suggest that although *PTPMT1* is not required for early activation of $CD8^+$ T cells, PTPMT1-mediated metabolism is important to sustain effector T cell specification and clonal expansion.

Consistent with the data obtained from *PTPMT1* KO cells, treatment of WT $CD8^+$ T cells with the PTPMT1-specific inhibitor alexidine dihydrochloride (AD) (*28*) produced a minimal effect on early activation. The formation of $CD25^+$ or $CD69^+$ $CD8^+$ T cells in the presence of AD was barely affected (Fig. 1, H to J). However, AD treatment inhibited the generation of IFN-γ–producing and granzyme B^+ effector cells in a dose-dependent manner (Fig. 1, H, K, and L). This effect was also associated with significantly reduced cell division (Fig. 1, H and M). These results suggest that the catalytic activity of PTPMT1 is necessary for its function in $CD8^+$ effector cell differentiation and expansion.

PTPMT1 deletion impairs $CD8^+$ T cell antitumor immunity

Given that *PTPMT1* was important for $CD8^+$ effector cell development, we evaluated the role of PTPMT1 in antitumor immunity. Naïve WT $CD45.2^+CD8^+$OT-I T cells that recognized an epitope derived from chicken ovalbumin (OVA) were cotransferred at the 1:1 ratio with naïve *PTPMT1* KO $CD45.2^+CD8^+$OT-I/$Thy1.1^+$ cells into congenic host BoyJ mice ($CD45.1^+$). The recipient mice were inoculated with OVA-expressing B16 melanoma cells 24 hours later. Percentages of donor-derived T cells in the peripheral blood, spleen, tumor, and tumor-draining lymph nodes (TDLNs) were determined 3 weeks after T cell adoptive transfer (Fig. 2, A and B). In this competitive setting, *PTPMT1* KO $CD8^+$OT-I/$Thy1.1^+$ T cells showed markedly reduced frequencies relative to WT $CD8^+$OT-I T cells, which dominated the overall immune response (Fig. 2, C and D), demonstrating that $CD8^+$ T cells lacking *PTPMT1* were defective in tumor antigen–stimulated responses.

$CD8^+$ T cells within the tumor microenvironment can differentiate into a dysfunctional/exhausted state, but a small subset of clonotypes in the exhausted T cell population are stem-like T cells that are responsible for the proliferative burst following immune checkpoint therapy (*2*–*4*). We examined cell compositions of tumor-infiltrating $CD8^+$ T cells and found that ~90% of *PTPMT1* KO $CD8^+$ T cells, in contrast to ~70% of WT control cells, expressed programmed cell death 1 (PD-1) and T cell membrane protein 3 (TIM3), markers of $CD8^+$ T cells in an exhausted state (Fig. 2, E and F). Moreover, the population of *PTPMT1* KO stem-like $CD8^+$ T cells ($PD\text{-}1^+Tcf1^+TIM3^-$) was reduced by 50% compared to the WT counterparts (Fig. 2, E and G). As *PTPMT1* KO tumor-infiltrating $CD8^+$ T cells were significantly reduced (Fig. 2H), the total number of KO exhausted $CD8^+$ T cells per gram of tumor tissue was decreased, and the total number of KO stem-like $CD8^+$ T cells was more markedly decreased compared to the WT counterparts (Fig. 2H). Furthermore, we analyzed donor-derived $CD8^+$ T cells in TDLNs. An increase in the percentage of KO exhausted $CD8^+$ T cells and a decrease in the percentage of KO stem-like $CD8^+$ T cells were also observed in TDLNs (Fig. 2, I to K). The absolute numbers of *PTPMT1* KO $CD8^+$ T cells in various functional states in TDLNs exhibited similar changes to those in the tumor microenvironment (Fig. 2L). These data highlight the critical role of PTPMT1 in preventing $CD8^+$ effector cell exhaustion and maintaining stem-like $CD8^+$ T cells.

We next asked whether *PTPMT1* deficiency affected $CD8^+$ T cell persistence and affected their long-term antitumor function. The OVA peptide (SIINFEKL)–activated WT and *PTPMT1* KO $CD8^+$OT-I/$Thy1.1^+$ T cells were adoptively transferred into

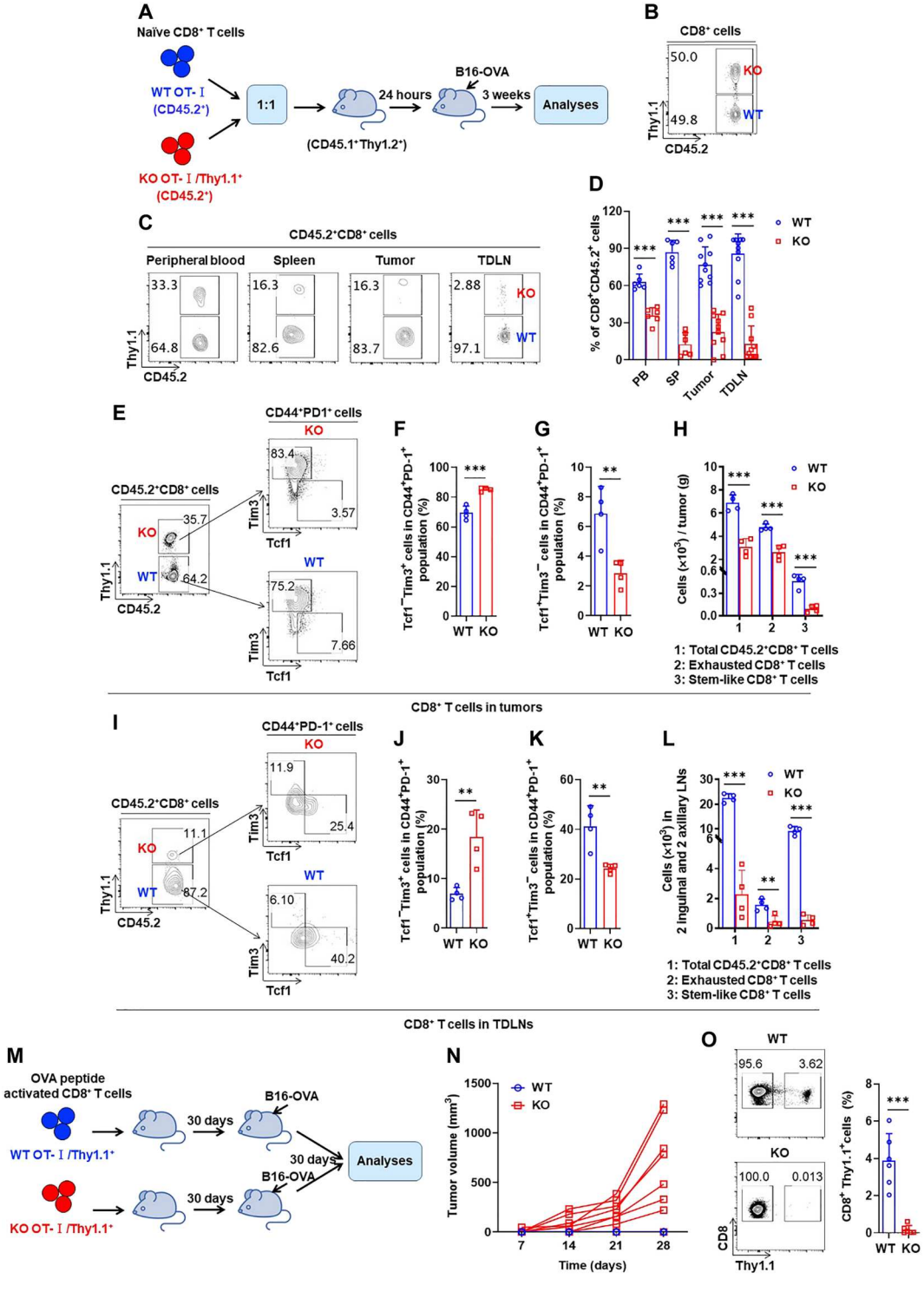

Fig. 2. *PTPMT1* deletion impairs CD8$^+$ T cell antitumor immunity. (**A** and **B**) CD8$^+$ T cells (5×10^5) isolated from WT OT-I mice (CD45.2$^+$) were mixed with CD8$^+$ T cells collected from *PTPMT1* KO OT-1/Thy1.1$^+$ mice (CD45.2$^+$) at the 1:1 ratio and adoptively transferred into congenic BoyJ mice (CD45.1$^+$). The recipient mice were subcutaneously injected 5×10^5 B16-OVA melanoma cells 24 hours later. The mice were euthanized 3 weeks later, and CD8$^+$ T cells in the peripheral blood (PB), spleen (SP), tumors, and TDLNs were examined. (**C** and **D**) Frequencies of WT and *PTPMT1* KO OT-I CD8$^+$ T cells in the donor-derived CD8$^+$ T cell population (CD45.2$^+$) in the peripheral blood, spleen, tumors, and TDLNs were determined. (**E** to **H**) Tumor-infiltrating lymphocytes (TILs) were isolated from tumors. Exhausted CD8$^+$ T cells (Tcf1$^-$Tim3$^+$CD44$^+$PD-1$^+$) [(E) and (F)] and stem-like CD8$^+$ T cells (Tcf1$^+$Tim3$^-$CD44$^+$PD-1$^+$) [(E) and (G)] in the donor-derived CD8$^+$ T cell population were analyzed by FACS analyses. Total cell numbers of donor-derived CD8$^+$ T cells, exhausted CD8$^+$ T cells, and stem-like CD8$^+$ T cells per gram of tumor tissue were determined (E and H). (**I** to **L**) Lymphocytes were isolated from TDLNs. Exhausted CD8$^+$ T cells [(I) and (J)] and stem-like CD8$^+$ T cells [(I) and (K)] in the donor-derived CD8$^+$ T cell population were analyzed as above. Total cell numbers of donor-derived CD8$^+$ T cells, exhausted CD8$^+$ T cells, and stem-like CD8$^+$ T cells in TDLNs were determined [(I) and (L)]. (**M** to **O**) OVA peptide–activated WT OT-I/Thy1.1$^+$ CD8$^+$ T cells or *PTPMT1* KO OT-I/Thy1.1$^+$ CD8$^+$ T cells (10×10^6) were adoptively transferred into BoyJ mice. The recipient mice were subcutaneously injected 5×10^5 B16-OVA melanoma cells 30 days later (M). Tumor growth was monitored at the indicated time points (N). Mice were euthanized, and frequencies of Thy1.1$^+$ CD8$^+$ T cells in TDLNs were examined by FACS analyses (O). Data are presented as means ± SD of biological replicates. $^{**}P < 0.01$ and $^{***}P < 0.001$.

congenic BoyJ mice separately, and OVA-expressing B16 cells were inoculated into these animals 30 days later (Fig. 2M). In this setting, all inoculated tumor cells were eliminated by WT donor CD8$^+$ T cells. In contrast, mice that received *PTPMT1* KO cells uniformly developed tumors of various sizes (Fig. 2N). Notably, *PTPMT1* KO CD8$^+$Thy1.1$^+$ T cells in TDLNs were completely undetectable (Fig. 2O). These data together suggest that PTPMT1-mediated metabolism is critical for CD8$^+$ T cell persistence and antitumor immunity.

To further determine the role of *PTPMT1* in CD8$^+$ T cell antitumor immunity, we adoptively transferred OVA peptide–activated CD8$^+$ T cells to congenic BoyJ mice with established B16-OVA

melanomas (Fig. 3A). *PTPMT1* KO CD8$^+$OT-I/Thy1.1$^+$ cells displayed a much lower ability to control tumor progression compared to WT control CD8$^+$OT-I/Thy1.1$^+$ cells (Fig. 3B). Although *PTPMT1* KO CD8$^+$ T cells had a similar efficiency in infiltrating into tumor masses as WT CD8$^+$ T cells (Fig. 3C and fig. S3A), IFN-γ–producing and granzyme B$^+$ effector CD8$^+$ T cells were greatly decreased in the *PTPMT1* KO tumor-infiltrating CD8$^+$ T cell population (Fig. 3D and fig. S3A). Furthermore, exhausted CD8$^+$ T cells were significantly increased, and stem-like CD8$^+$ T cells were decreased by 70% in the *PTPMT1* KO tumor-infiltrating CD8$^+$ T cell population compared to those in the WT counterparts (Fig. 3, E and F, and fig. S3A), although *PTPMT1* expression levels were similar in WT stem-like CD8$^+$ T cells and exhausted CD8$^+$ T cells (Fig. 3G). We also examined donor-derived CD8$^+$ T cells in

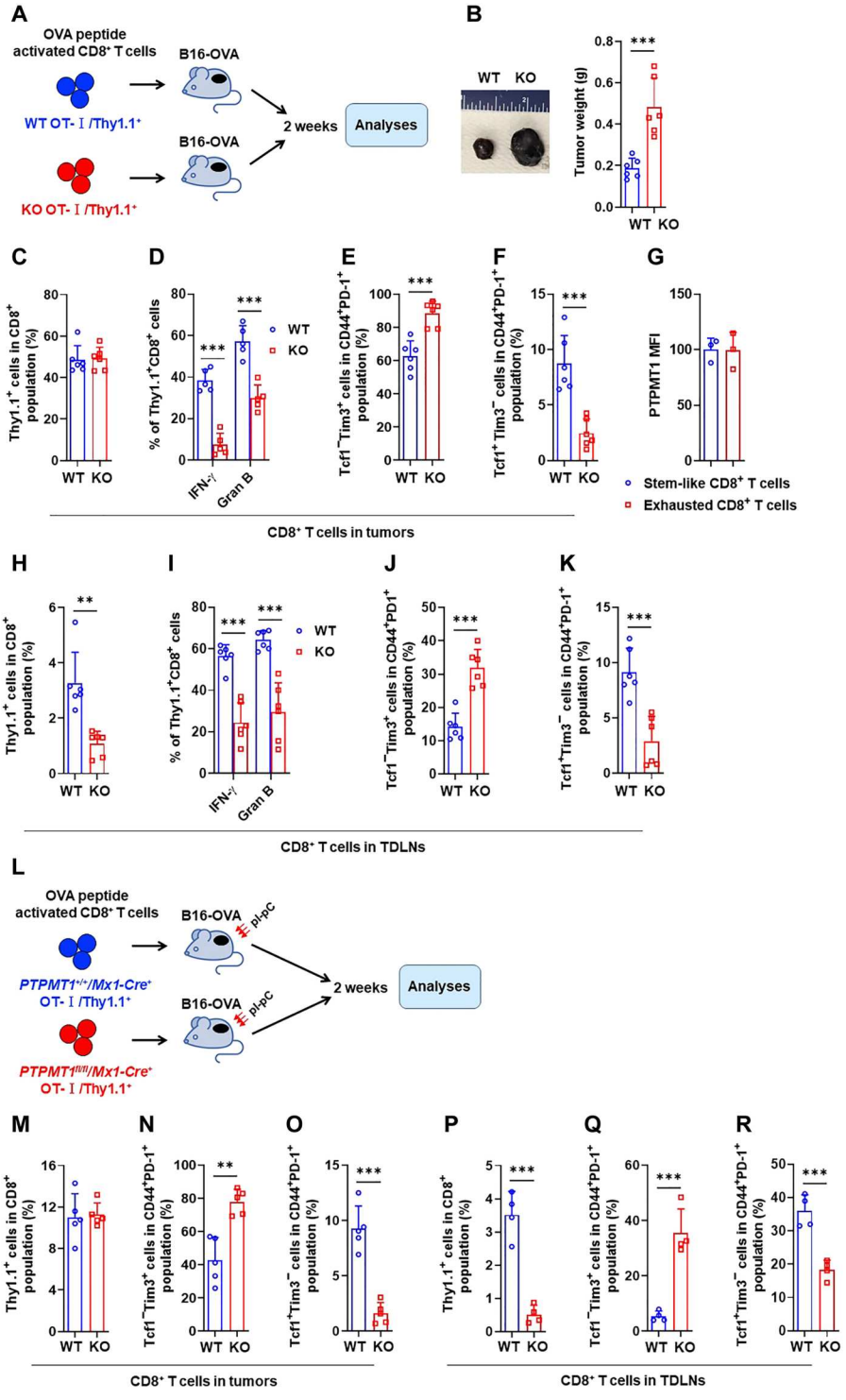

Fig. 3. *PTPMT1* loss accelerates CD8$^+$ T exhaustion and impairs stem-like CD8$^+$ T cell maintenance in tumors and TDLNs. (**A** to **F**) B16-OVA melanoma cells (5×10^5) were subcutaneously injected into Boy J mice to allow tumor development for 10 days. OVA peptide–activated WT OT-I/Thy1.1$^+$ CD8$^+$ T cells or *PTPMT1* KO OT-I/Thy1.1$^+$ CD8$^+$ T cells (10×10^6) were adoptively transferred into the tumor-bearing mice (A). Mice were euthanized 14 days after T cell transfusion, and tumor weights were assessed (B). Tumor-infiltrating lymphocytes (TILs) were isolated from tumors and frequencies of total donor-derived CD8$^+$ T cells (Thy1.1$^+$) (C), effector CD8$^+$ T cells (Thy1.1$^+$IFN-γ$^+$ or Thy1.1$^+$granzyme B$^+$) (D), exhausted CD8$^+$ T cells (Tcf1$^-$Tim3$^+$CD44$^+$PD-1$^+$) (E), and stem-like CD8$^+$ T cells (Tcf1$^+$Tim3$^-$CD44$^+$PD-1$^+$) (F) in the donor-derived CD8$^+$ T cell population were determined by FACS analyses. (**G**) WT donor-derived exhausted CD8$^+$ T cells and stem-like CD8$^+$ T cells were analyzed for PTPMT1 levels by intracellular immunostaining, followed by FACS analyses. MFI, mean fluorescence intensity. (**H** to **K**) Lymphocytes isolated from TDLNs were analyzed for donor-derived CD8$^+$ T cells (H), and effector CD8$^+$ T cells (I), exhausted CD8$^+$ T cells (J), and stem-like CD8$^+$ T cells (K) in the donor-derived CD8$^+$ T cell population as above. (**L**) CD8$^+$ T cells isolated from *PTPMT1*$^{fl/fl}$/*Mx1-Cre*$^+$/OT-I/Thy1.1$^+$ (KO) and *PTPMT1*$^{+/+}$/*Mx1-Cre*$^+$/OT-I/Thy1.1$^+$ (WT) control mice were activated with OVA peptide. Activated CD8$^+$ T cells were adoptively transferred to BoyJ mice with established B16-OVA melanomas as above. Recipient mice were administered by intraperitoneal injection of three doses of pI-pC (1.0 μg/g of body weight) every other day over 5 days to induce Cre expression and *PTPMT1* deletion from *PTPMT1*$^{fl/fl}$/*Mx1-Cre*$^+$ OT-I/Thy1.1$^+$ donor-derived T cells. CD8$^+$ T cells from tumors (**M** to **O**) and TDLNs (**P** to **R**) were examined as above. Data are presented as means ± SD of biological replicates. $^{**}P < 0.01$ and $^{***}P < 0.001$.

TDLNs. The percentage of *PTPMT1* KO CD8$^+$Thy1.1$^+$ T cells was much lower than that of WT control cells (Fig. 3H and fig. S3B). KO IFN-γ–producing and granzyme B$^+$ effector cells were decreased by half (Fig. 3I and fig. S3B). An increase in exhausted KO CD8$^+$ T cells and a decrease in KO stem-like CD8$^+$ T cells were also evident in TDLNs (Fig. 3, J and K, and fig. S3B). These findings are fully consistent with the results obtained from naïve CD8$^+$ T cell transfer experiments (Fig. 2, A to K).

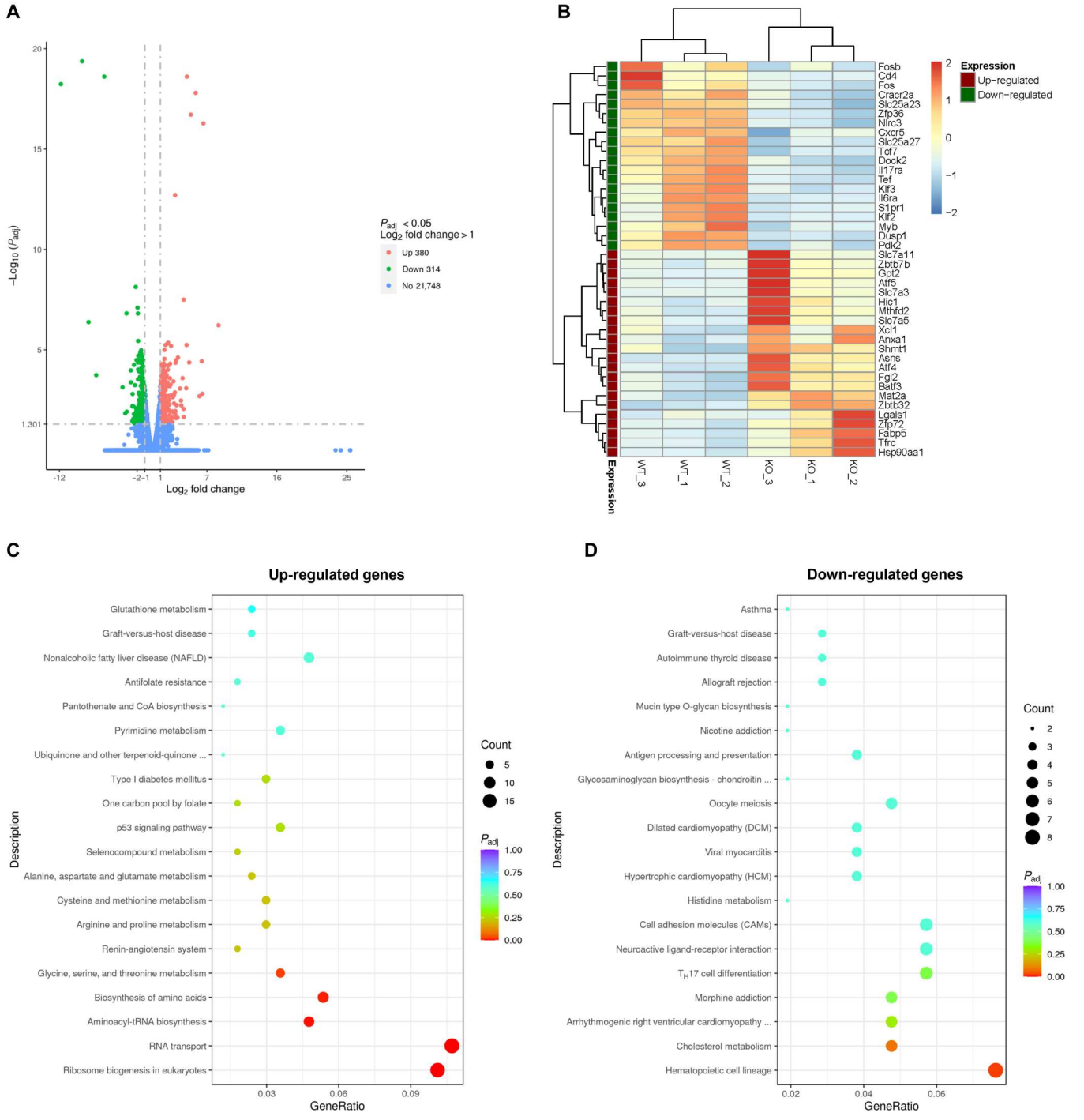

Fig. 4. Adaptive transcriptomic responses to *PTPMT1* depletion in activated CD8$^+$ T cells. CD8$^+$ T cells isolated from *PTPMT1* KO and WT control mice were activated by CD3/CD28 antibodies. The cells were harvested and processed for RNA-seq analyses. (**A**) A volcano plot of differentially expressed genes. Three hundred eighty significantly up-regulated genes (red) and 314 significantly down-regulated genes (green) in *PTPMT1* KO cells ($P < 0.05$, fold changes > 2) were identified. (**B**) Heatmap showing representative differentially expressed genes. The color bar indicates the *Z* score. (**C** and **D**) Enriched Kyoto Encyclopedia of Genes and Genomes (KEGG) pathways for up-regulated genes (C) and down-regulated genes (D) in *PTPMT1* KO CD8$^+$ T cells.

Constitutive *PTPMT1* depletion from naïve CD8$^+$ cells inhibited the development of effector cells, which could affect the development of subsequent subpopulations. We therefore investigated the effects of *PTPMT1* depletion after CD8$^+$ effector T cell expansion. To this end, we generated inducible *PTPMT1* KO mice (*PTPMT1*$^{fl/fl}$/*Mx1-Cre*$^+$) through the crossbreeding of *PTPMT1*$^{fl/+}$ mice (*20*) and *Mx1-Cre*$^+$ mice (*29*). The *Mx1-Cre*$^+$ mice express the DNA recombinase Cre in the entire hematopoietic system, including T cells, upon polyinosinic-polycytidylic acid (pI-pC) administration. *PTPMT1*$^{fl/fl}$/*Mx1-Cre*$^+$ mice were then crossed with OT-I mice. CD8$^+$ T cells were isolated from untreated *PTPMT1*$^{fl/fl}$/*Mx1-Cre*$^+$/OT-I/Thy1.1$^+$ and *PTPMT1*$^{+/+}$/*Mx1-Cre*$^+$/OT-I/Thy1.1$^+$ control mice and activated with OVA peptide. The activated CD8$^+$ T cells were adoptively transferred into BoyJ mice with established B16-OVA melanomas, followed by pI-pC administration to induce Cre expression and *PTPMT1* deletion specifically in *PTPMT1*$^{fl/fl}$/*Mx1-Cre*$^+$/OT-1/Thy1.1$^+$ donor-derived T cells. CD8$^+$ T cells isolated from tumors and TDLNs were examined as described above (Fig. 3L). No differences in the total donor-derived CD8$^+$ T cells in tumors were observed between WT and *PTPMT1* KO groups (Fig. 3M and fig. S3C). However, *PTPMT1* KO exhausted CD8$^+$ T cells (Fig. 3N and fig. S3C), and stem-like CD8$^+$ T cells (Fig. 3O and fig. S3C) exhibited a significant increase and decrease, respectively, compared to the WT counterparts. In TDLNs, donor-derived CD8$^+$ T cells were greatly decreased in the *PTPMT1* KO group (Fig. 3P and fig. S3D), but similar trends in KO exhausted CD8$^+$ T cells (Fig. 3Q and fig. S3D) and KO stem-like CD8$^+$ T cells (Fig. 3R and fig. S3D) were observed, further confirming the crucial role of *PTPMT1* in the prevention of CD8$^+$ effector cell exhaustion and the maintenance of stem-like CD8$^+$ T cells.

PTPMT1 is essential for CD8$^+$ T cell responses to lymphocytic choriomeningitis virus infection

To further assess the effects of *PTPMT1* depletion on CD8$^+$ T cells, we infected *PTPMT1* KO (*PTPMT1*$^{fl/fl}$/*Lck-Cre*$^+$) and WT control (*PTPMT1*$^{+/+}$/*Lck-Cre*$^+$) mice with murine lymphocytic choriomeningitis viruses (LCMVs) (strain Armstrong), which caused acute infection (*30*). Responses of CD8$^+$ T cells in the peripheral blood and spleen were examined at day 8. LCMV antigen–specific effector CD8$^+$ T cells (CD8$^+$CD44$^+$GP33$^+$ and CD8$^+$CD44$^+$GP276$^+$) were markedly decreased in the peripheral blood (fig. S4, A and B) and spleen (fig. S4, C and D) in *PTPMT1* KO mice. These results reaffirm the critical role of PTPMT1 in CD8$^+$ T cell immune responses.

Adaptive transcriptomic responses to *PTPMT1* loss in activated CD8$^+$ T cells

To delineate the molecular mechanisms underlying the profound defects of *PTPMT1*-depleted CD8$^+$ T cells, we determined the transcriptomic profiles of activated *PTPMT1* KO and WT CD8$^+$ T cells by RNA sequencing (RNA-seq) analyses. Six hundred ninety-four differentially expressed genes were identified; 380 genes were up-regulated (Fig. 4A, red) and 314 genes were down-regulated (Fig. 4A, green) in KO cells. Many transcriptional factors were differentially expressed in KO cells, including those of the bZip family (*Atf4*, *Atf5*, *Fos*, *Fosb*, *Tef*, and *Batf3*) and zinc finger proteins (*Klf2*, *Klf3*, *Hic1*, *Zbtb7b*, *Zbtb32*, *Zfp36*, and *Zfp72*) (Fig. 4B). Some of these transcriptional factors are known to be involved in T cell immune responses (*31*–*34*). Additional transcriptional factors down-regulated in *PTPMT1* KO CD8$^+$ T cells include transcription factor 7 (*Tcf7*) (Tcf1) and *Myb*, which are critical for the formation and function of stem-like CD8$^+$ T cells (*5*, *35*, *36*). *CXCR5*, a chemokine receptor and a marker for stem-like CD8$^+$ T cells (*3*, *6*, *37*), was also noticeably down-regulated in *PTPMT1* KO cells. Other genes (*Xcl1*, *Tfrc*, *Anxa1*, *Nlrc3*, *Il6ra*, *Dock2*, *Fgl2*, *Dusp1*, *Hsp90aa1*, *Cracr2a*, and *Lgals1*) related to T cell activation were also affected by *PTPMT1* deletion. In addition, *PTPMT1* KO cells exhibited down-regulation of *S1pr1*, a receptor that regulates the egress of lymphocytes from the thymus and peripheral lymphoid organs to the circulation (*38*). KO CD8$^+$ effector T cells exhibited reduced chemotaxis to sphingosine-1-phosphate (S1P) compared to WT control cells (fig. S5), suggesting that the diminished mobilization of *PTPMT1* KO CD8$^+$ T cells from lymph nodes during the immune response is an additional possible mechanism contributing to impaired antitumor immunity. In contrast, a series of solute carrier family members were up-regulated in *PTPMT1* KO cells, including those of the mitochondrial carrier family (*Slc25a23* and *Slc25a27*) and cationic amino acid transporter/glycoprotein-associated amino acid transporter family (*Slc7a3*, *Slc7a5*, and *Slc7a11*), indicating increased amino acid uptakes in the KO cells. Genes that are involved in the one-carbon metabolic pathway (*Shmt1*, *Mthfd2*, and *Mat2a*) were also up-regulated in *PTPMT1* KO cells, implying adaptively enhanced folic acid metabolism. In keeping with these observations, pathway enrichment analyses of up-regulated genes highlighted categories such as amino acid metabolism, one-carbon metabolism, glutathione metabolism, pyrimidine metabolism, p53 signaling pathway, etc. (Fig. 4C). Genes related to autoimmune disease, antigen processing and presentation, T helper 17 (T_H17) cell differentiation, etc., were down-regulated (Fig. 4D). These adaptive or secondary gene expression responses are consistent with the phenotypic and functional changes in *PTPMT1* KO cells, providing additional support for the critical role of PTPMT1-mediated metabolism in CD8$^+$ T cells.

PTPMT1 deficiency inhibits mitochondrial metabolism and causes bioenergetic stress

Given that PTPMT1 is localized to the mitochondrial inner membrane where oxidative phosphorylation and ATP synthesis take place, we sought to determine the fundamental impact of *PTPMT1* ablation on mitochondria and cellular metabolism in CD8$^+$ effector cells (CD8$^+$CD44$^+$). The loss of *PTPMT1* did not affect overall mitochondrial content in the KO cells according to the copy numbers of mitochondrial DNA (Fig. 5A) and the mitochondria staining results (Fig. 5B). Moreover, glucose uptake was not significantly changed in *PTPMT1* KO cells (Fig. 5C). Steady-state total cellular ATP levels in *PTPMT1* KO cells were comparable to those in WT control cells (Fig. 5D). We then assessed mitochondrial aerobic metabolism in activated CD8$^+$ T cells with full access to all metabolic substrates, by real-time measurement of oxygen consumption under basal conditions, in the presence of the mitochondrial inhibitor oligomycin, the mitochondrial uncoupling compound carbonyl cyanide *p*-trifluoromethoxyphenylhydrazone (FCCP), and the respiratory chain inhibitor rotenone. Compared to WT cells, *PTPMT1* KO cells displayed much lower basal oxygen consumption rates (OCRs) and maximal oxidative capacity (Fig. 5E). Measurement of extracellular proton flux showed that *PTPMT1*-depleted cells had slightly increased basal extracellular acidification rates (ECARs) (Fig. 5F). In response to the mitochondrial inhibition by oligomycin, ECARs were further elevated in WT

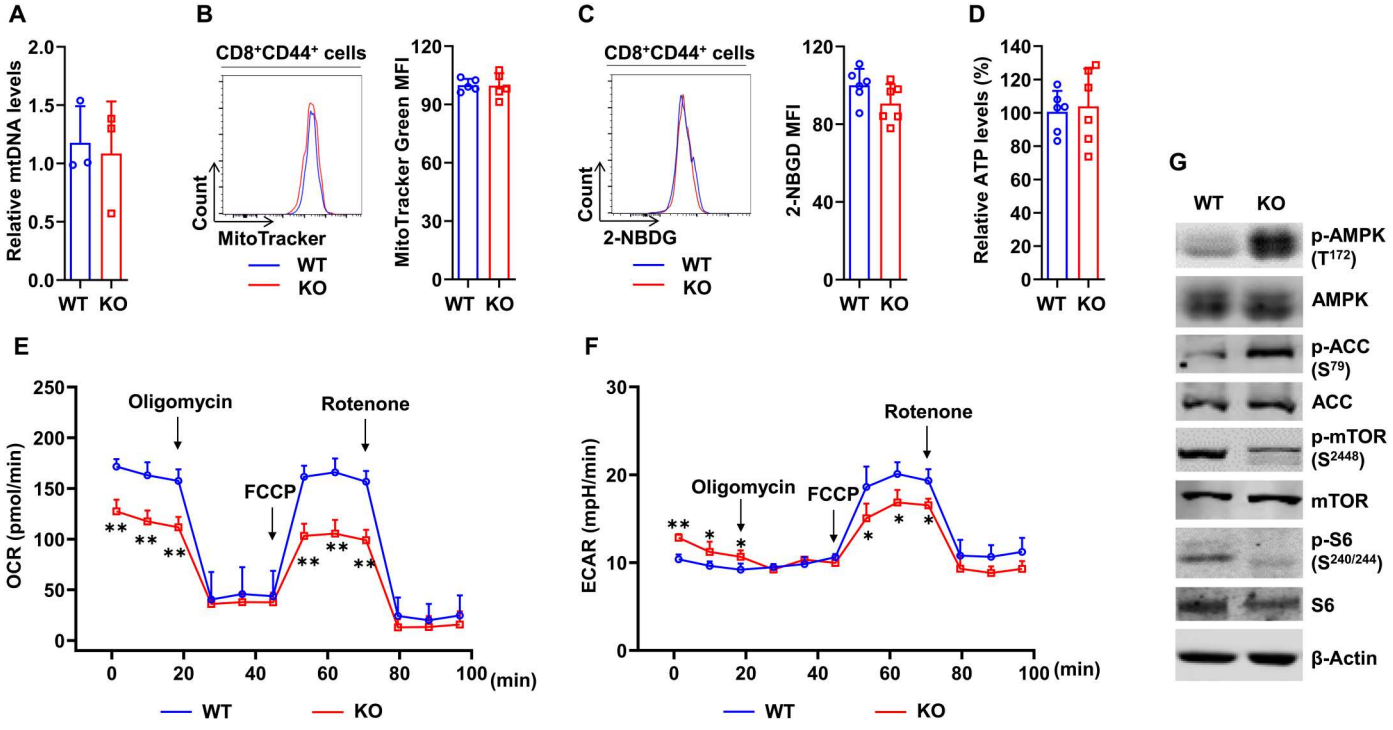

Fig. 5. PTPMT1 ablation induces mitochondrial metabolism inhibition and bioenergetic stress. CD8$^+$ T cells isolated from *PTPMT1* KO and WT control mice were activated by CD3/CD28 antibodies. (**A**) Total DNA was extracted. Mitochondrial content was estimated by comparing mitochondrial DNA (mtDNA; cytochrome B) levels to genomic DNA (18*S* ribosomal gene) levels by quantitative polymerase chain reaction. (**B**) Cells were stained with MitoTracker Green (100 nM) followed by FACS analyses for MFI in the activated CD8$^+$CD44$^+$ population. (**C**) Cells were incubated with 2-(*N*-(7-nitrobenz-2-oxa-1,3-diazol-4-yl)amino)-2-deoxyglucose (2-NBDG) (200 μM) (Thermo Fisher Scientific) at 37°C for 30 min and washed with PBS, followed by FACS analyses for MFI in the CD8$^+$CD44$^+$ population. (**D**) Total cellular ATP levels were assessed using a CellTiter-Glo 2.0 cell viability assay kit (Promega), which is a homogeneous method to quantify cellular ATP. (**E** and **F**) OCR (E) and ECAR (F) of the activated CD8$^+$ T cells ($n = 3$ mice per group) in the medium containing all metabolic substrates were measured by a Seahorse metabolic flux analyzer in the presence of the mitochondrial inhibitor (oligomycin), the uncoupling agent (FCCP), and the respiratory chain inhibitor (rotenone). Data are presented as means ± SD of biological replicates. *$P < 0.05$ and **$P < 0.01$. (**G**) Activated CD8$^+$ T cells were lysed, and whole-cell lysates were examined by immunoblotting with the indicated antibodies. Representative results from three mice per group are shown.

cells conceivably due to the diversion of pyruvate from oxidation in the mitochondrion to fermentation in the cytosol. However, this response was dampened in *PTPMT1*-depleted cells, indicating that pyruvate was already largely reduced to lactate under basal conditions.

Despite total cellular ATP levels being maintained (Fig. 5D), adenosine 5′-monophosphate–activated protein kinase (AMPK), a master cellular energy stress sensor (*39*), was highly activated in *PTPMT1* KO cells as determined by the phosphorylation of Thr^{172} (Fig. 5G). Acetyl–coenzyme A (CoA) carboxylase, one of the targets of AMPK and a negative regulator of fatty acid oxidation (*40*), was inhibited, as evidenced by the increase in the inhibitory phosphorylation of the enzyme (Fig. 5G), implying that fatty acid metabolism was enhanced in *PTPMT1* KO cells. In agreement with previous findings that AMPK negatively regulates mammalian target of rapamycin (mTOR) signaling (*41*, *42*), mTOR was substantially inhibited in *PTPMT1*-deleted cells (Fig. 5G). The activity of S6 ribosomal protein, a key downstream component of mTOR signaling, was also concomitantly decreased, demonstrating diminished anabolic activities in the KO cells (Fig. 5G).

Loss of PTPMT1 limits mitochondrial utilization of pyruvate

To gain further insights into the acting mechanisms of PTPMT1, we measured respiratory responses of PTPMT1-deficient mitochondria to single, specific metabolic substrates. These assays required a large number of mitochondria. Therefore, we isolated mitochondria from the liver of *PTPMT1*$^{fl/fl}$/*Mx1-Cre*$^+$ mice and *PTPMT1*$^{+/+}$/*Mx1-Cre*$^+$ control mice and used hepatocyte mitochondria to assess ATP synthesis–driven oxygen consumption. The *Mx1-Cre* transgene expresses the DNA recombinase Cre in the liver at the same efficiency as that in the hematopoietic system upon pI-pC administration (*29*). As shown in Fig. 6A, in the presence of pyruvate, the major substrate of mitochondria and a key metabolite derived from glucose, ATP synthesis–driven oxygen consumption was remarkably decreased in PTPMT1 null mitochondria, suggesting that pyruvate utilization was impaired. In contrast, oxygen consumption of these same mitochondria was enhanced when fatty acids were supplied as the fuel, verifying enhanced fatty acid oxidation (Fig. 6B). In addition, increased respiratory responses were observed in PTPMT1-ablated mitochondria when glutamate was provided (Fig. 6C). Directly feeding the mitochondria with succinate, the substrate of complex II in the electron transport chain, produced comparable OCRs in PTPMT1 null and WT control mitochondria (Fig. 6D), demonstrating the intact functionality of the electron transport chain in PTPMT1-deficient mitochondria. Since mitochondrial pyruvate transporters/carriers

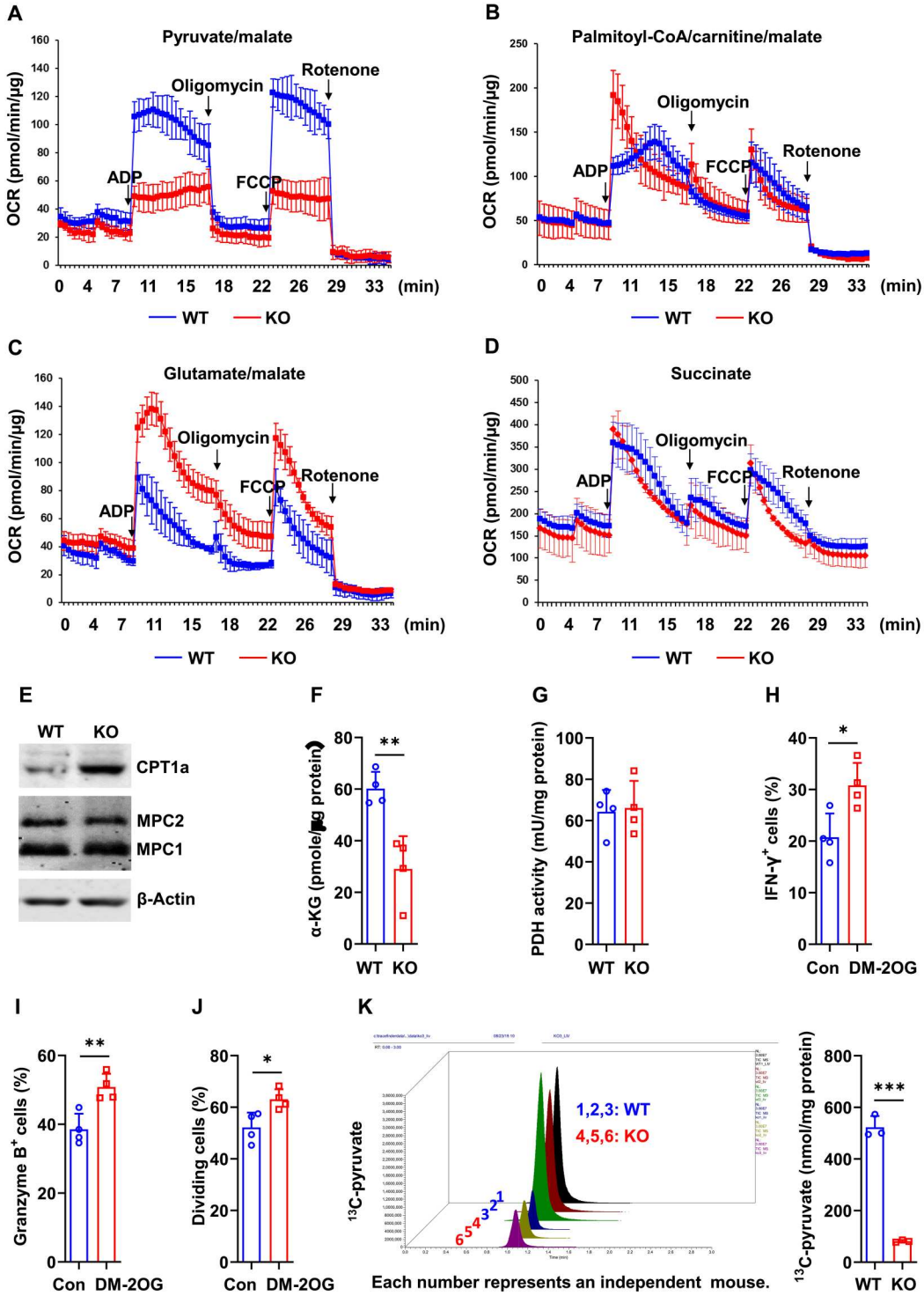

Fig. 6. PTPMT1 deficiency limits mitochondrial utilization of pyruvate. (**A** to **D**) Mitochondria were isolated from livers dissected from *PTPMT1*$^{fl/fl}$/*Mx1-Cre*$^{+}$ mice and *PTPMT1*$^{+/+}$/*Mx1-Cre*$^{+}$ littermates ($n = 3$ mice per group) 2 weeks following pI-pC administration and *PTPMT1* deletion. Oxygen consumption of the mitochondria was measured in the presence of pyruvate/malate (A), palmitoyl-CoA/carnitine/malate (B), glutamate/malate (C), or succinate (D), following the addition of adenosine 5′-diphosphate (ADP), oligomycin, FCCP, and rotenone. (**E**) CD8^{+} T cells isolated from *PTPMT1*$^{fl/fl}$/*Lck-Cre*$^{+}$ mice and *PTPMT1*$^{+/+}$/*Lck-Cre*$^{+}$ littermates were activated by CD3/CD28 antibodies. Whole-cell lysates were prepared and examined by immunoblotting with the indicated antibodies. Representative results from three mice per group are shown. α-KG levels (**F**) and PDH activities (**G**) in the lysates were measured using an α-KG assay kit and a PDH activity colorimetric assay kit (BioVision) following the manufacturer's instructions. (**H** to **J**) CD8^{+} T cells isolated from *PTPMT1* KO mice were activated with CD3/CD28 antibodies in the presence of cell permeable α-KG [dimethyl-ketoglutarate, DM-2OG (4 mM)] or vehicle control. Cells were harvested and analyzed for IFN-γ (H), granzyme B (I), and cell division (J) by FACS analyses. (**K**) Mitochondria were isolated as described in (A). They were assessed by the pyruvate uptake assay. ^{13}C-pyruvate levels in the mitochondrial lysates were measured by mass spectrometry. Data are presented as means ± SD of biological replicates. *P < 0.05, **P < 0.01, and ***P < 0.001.

MPC1 and *MPC2* were equally expressed in *PTPMT1* KO and WT CD8^{+} T cells (Fig. 6E), these results suggest that the substrate utilization of KO mitochondria was shifted from pyruvate to fatty acids and glutamate. Expression of CPT1a, an essential enzyme regulating fatty acid metabolism, was greatly increased in *PTPMT1* KO cells (Fig. 6E), suggesting elevated activation of fatty acid partitioning/transport into the mitochondrion in *PTPMT1* KO cells.

We also examined α-ketoglutarate (α-KG), an important metabolite in the tricarboxylic acid (TCA) cycle that is supported by extramitochondrial pyruvate, and found that α-KG levels were decreased in *PTPMT1* KO CD8^{+} T cells (Fig. 6F). Notably, the activity of pyruvate dehydrogenase (PDH), the enzyme that catalyzes the conversion of pyruvate into acetyl-CoA to feed the TCA cycle, was not affected by PTPMT1 deficiency (Fig. 6G). Moreover, the

addition of cell permeable dimethyl 2-oxoglutarate (DM-2OG) to T cell activation medium partially rescued the production and expansion of effector cells in *PTPMT1* KO CD8$^+$ T cells (Fig. 6, H to J), suggesting that the functional defects observed in *PTPMT1* KO CD8$^+$ T cells were attributed, at least in part, to reduced levels of mitochondrial α-KG and decreased activity of the TCA cycle. These results, combined with the observation that *MPC1* and *MPC2* were equally expressed in *PTPMT1* KO and WT CD8$^+$ T cells (Fig. 6E), suggest that pyruvate import into the mitochondrion was diminished in the absence of PTPMT1. Further, ^{13}C-pyruvate uptake measurement by mass spectrometry confirmed that pyruvate uptake of PTPMT1 null mitochondria was decreased by >80% compared to that of WT mitochondria (Fig. 6K). These mechanistic data strongly support that the fuel selection of the mitochondria lacking PTPMT1 was shifted, leading to metabolic inflexibility.

Cellular metabolism is reprogrammed in *PTPMT1*-depleted CD8$^+$ T cells

To further elucidate the effects of *PTPMT1* loss on cell metabolism, we performed comprehensive metabolomic profiling for activated CD8$^+$ T cells. One hundred sixteen metabolites were measured with capillary electrophoresis mass spectrometry. The analyses showed that several metabolic pathways in *PTPMT1* KO cells were affected (Fig. 7, A and B). Levels of glucose 6-phosphate (G6P), fructose 6-phosphate (F6P), fructose 1,6-diphosphate (F1,6P), 2-phosphoglyceric acid (2PG), and pyruvate in the glycolytic pathway in the cytosol increased in these cells (Fig. 7C and fig. S6A). However, succinic acid, fumaric acid, and malic acid, which are the metabolites in the payoff phase of the TCA cycle in the mitochondrion, were reduced in the KO cells (Fig. 7C and fig. S6B). The disruption of the TCA cycle further supports that pyruvate utilization by the mitochondrion was diminished in the absence of PTPMT1. The pentose phosphate pathway, which plays an integral role in producing the reduced form of nicotinamide adenine dinucleotide phosphate (NADPH) and the five-carbon sugar ribose for purine synthesis, was also attenuated in *PTPMT1* KO cells, as demonstrated by decreases in ribulose 5-phosphate (Ru5P), ribose 5-phosphate (R5P), ribose 1-phosphate (R1P), and phosphoribosyl pyrophosphate (PRPP) levels (Fig. 7C and fig. S6C). The decrease in the pentose phosphate pathway appears to occur primarily at the G6P to R5P conversion, the first and a bottleneck reaction in the pentose phosphate pathway, since the G6P/R5P ratio was markedly increased in these cells (fig. S6C). Adenylate energy charge, an indicator of cellular energy status, was doubled in the KO cells (fig. S6B), suggesting that the utilization of energy for biochemical processes was decreased, consistent with greatly reduced anabolic activities in these cells. In addition, the glutathione (reduced form)/oxidized glutathione (GSH/GSSG) ratio, the primary determinant of the cellular redox state, decreased by half (fig. S6D), indicating oxidative stress in *PTPMT1*-deleted cells.

PTPMT1 deficiency induces oxidative stress and apoptosis in activated CD8$^+$ T cells

In alignment with the observation that fatty acid oxidation was enhanced in *PTPMT1* KO CD8$^+$ effector T cells (Figs. 5G and 6, B and E), lipid droplets detected in these cells were doubled as compared to those in WT control cells (Fig. 8A). Given these observations, we next sought to address how excessive fatty acid oxidation affected *PTPMT1* KO CD8$^+$ T cells. Oxidation of fatty acids in mitochondria yields much more ATP relative to carbohydrates (via pyruvate); however, fatty acid oxidation requires a greater rate of oxygen consumption for a given rate of ATP synthesis than carbohydrates. As a result, the by-product reactive oxygen species (ROS) are increased when mitochondria switch to fatty acids for energy metabolism. We examined ROS in CD8$^+$CD44$^+$ effector cells following 3 days of activation with 2′,7′-dichlorodihydrofluorescein diacetate (DCFDA) and found that *PTPMT1* KO cells had elevated overall cellular ROS levels (Fig. 8B), consistent with significantly decreased GSH/GSSG ratio in the KO cells (fig. S6D). In addition, mitochondrial superoxide as detected by MitoSOX was increased in these cells (Fig. 8C) [ROS levels in KO cells at day 1 of activation were also elevated (fig. S7A)]. Consistent with the role of ROS (at low or median levels) in driving cell cycle entry, KO cells exhibited a loss of quiescence and an increased G_1 phase. However, no differences in the G_2-M phase were observed between WT and *PTPMT1* KO cells (fig. S7B), suggesting that while the entry into the cell cycle was increased in *PTPMT1* KO cells, they were subsequently delayed in the G_1 phase. Persistently elevated oxidative stress can induce DNA damage and cell death. DNA damage determined by phosphorylation of H2A histone family member X (γ-H2AX) immunostaining was increased in *PTPMT1* KO cells (Fig. 8D), and apoptosis in *PTPMT1* KO cells was doubled compared to that in WT control cells (Fig. 8E). Consistent with the apoptosis data, B-cell lymphoma 2 (Bcl-2) levels were reduced in the KO cells (Fig. 8F). We also examined ROS levels and apoptosis in tumor-infiltrating CD8$^+$ T cells. Similar results were obtained. Although mitochondrial content was maintained (fig. S8A), ROS levels (fig. S8B) and apoptosis (fig. S8C) were elevated in *PTPMT1* KO CD8$^+$ T cells compared to those in the WT counterparts in the tumor microenvironment.

In addition, since AMPK was highly activated in *PTPMT1* KO cells (Fig. 5G), to investigate the relationship between AMPK activation, reduced pyruvate utilization in mitochondria, and elevated ROS levels, we treated *PTPMT1* KO cells with the AMPK inhibitor dorsomorphin. The inhibition of AMPK partially restored mitochondrial utilization of pyruvate (Fig. 8G) and reduced ROS levels by 50% (Fig. 8H). These findings suggest that the hyperactivation of AMPK hindered mitochondrial utilization of pyruvate, thus establishing a feedback loop that exacerbated the mitochondrial substrate switch and further elevated ROS levels. To determine whether increased ROS levels were responsible for enhanced apoptosis, decreased cell division, and impaired effector cell development in *PTPMT1* KO CD8$^+$ T cells, we treated KO cells with the ROS scavenging antioxidant *N*-acetylcysteine (NAC). NAC treatment effectively reversed apoptosis caused by *PTPMT1* deficiency (Fig. 8I). Moreover, cell division (Fig. 8J) and effector T cell production (Fig. 8, K and L) were largely rescued by NAC treatment, verifying that impaired *PTPMT1* KO CD8$^+$ T cells were attributable to oxidative stress.

Mitochondrial oxidation of pyruvate is essential for CD8$^+$ effector cell development

Pyruvate is transported into the mitochondrion through the transporter MPC. The MPC hetero-oligomeric complex is composed of two subunits (MPC1 and MPC2). Deletion of either subunit causes loss of another one of the complex (*43*, *44*) as both MPC1 and MPC2 are required for the stability and activity of the MPC complex (*45*, *46*). To determine whether decreased mitochondrial

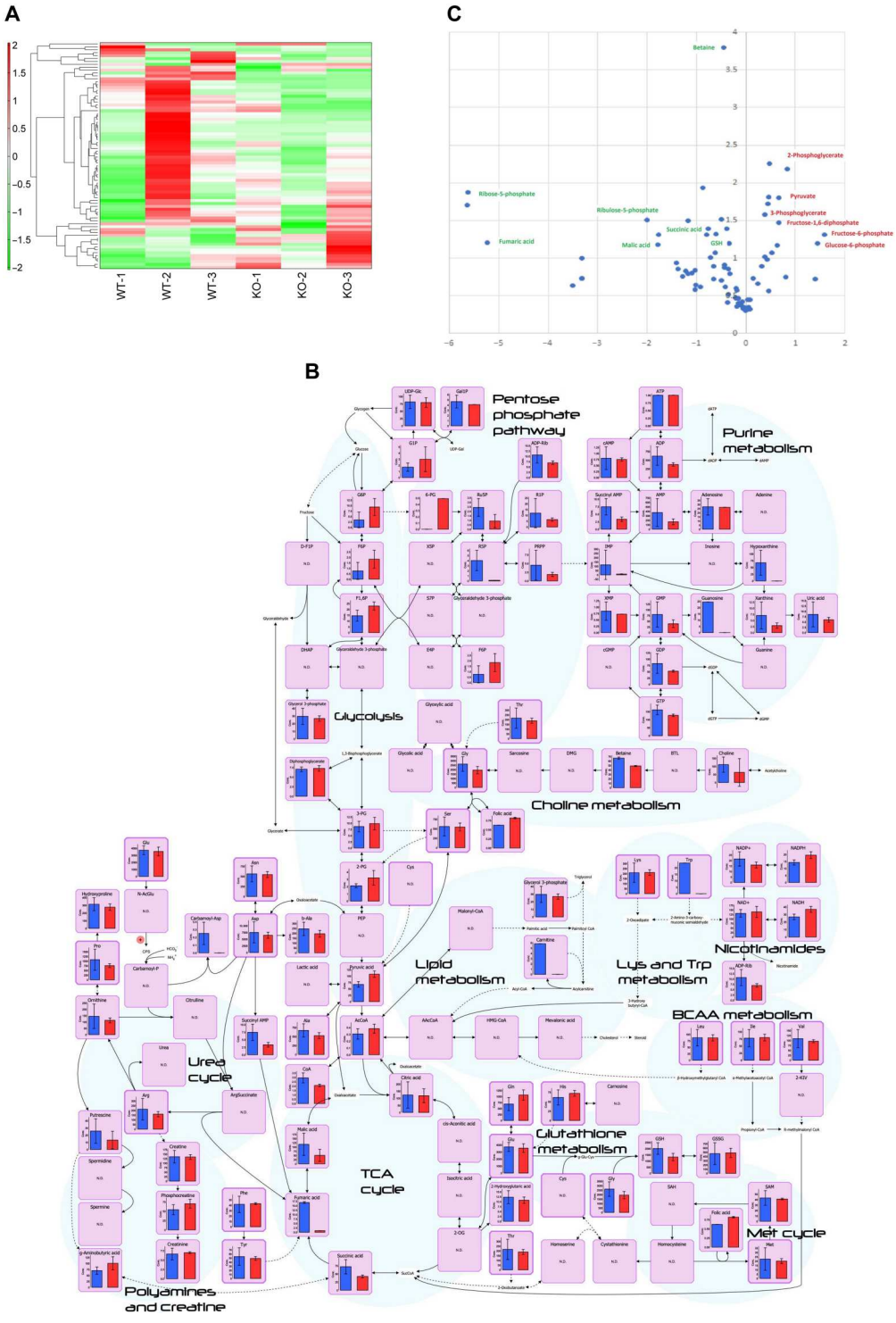

Fig. 7. Reprogrammed cellular metabolism in *PTPMT1* deleted CD8$^+$ effector T cells. CD8$^+$ T cells isolated from *PTPMT1* KO and WT control mice (n = 3 mice per group) were activated with CD3/CD28 antibodies. The cells were harvested and processed for metabolomic profiling using capillary electrophoresis time-of-flight mass spectrometry and capillary electrophoresis-triple quadrupole mass spectrometry. (**A**) Results of hierarchical clustering analyses of metabolite levels. (**B**) Changes in major metabolic pathways, including glycolysis, the TCA cycle, the pentose phosphate pathway, etc. N.D. indicates that the metabolites were not detected. (**C**) A volcano plot of significantly up-regulated (red) and down-regulated (green) metabolites.

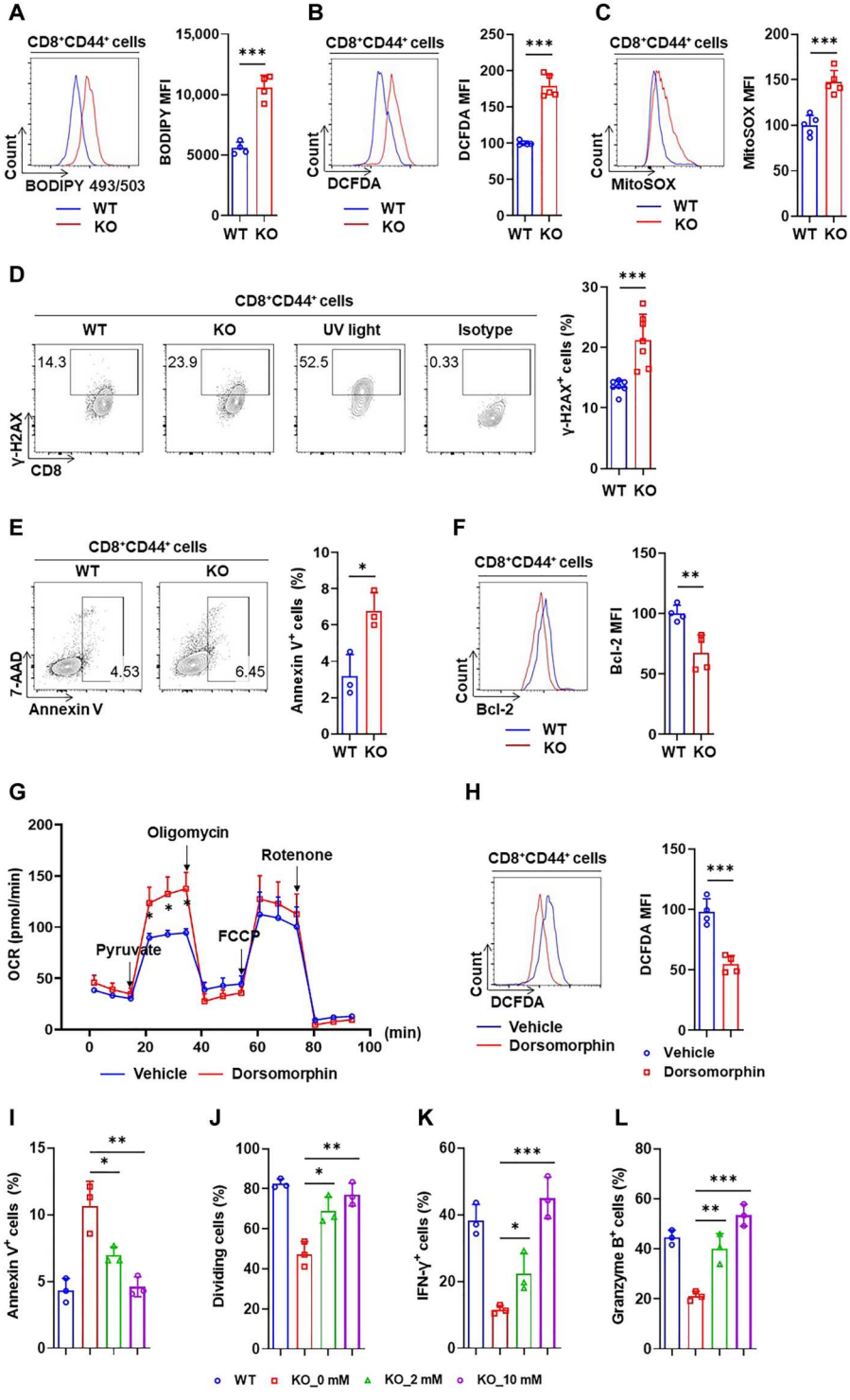

Fig. 8. Defective CD8$^+$ effector T cell development induced by *PTPMT1* depletion is attributable to oxidative stress and apoptosis. WT and *PTPMT1* KO CD8$^+$ T cells were activated by CD3/CD28 antibodies and then stained with BODIPY 493/503 (**A**), DCFDA (**B**), and MitoSOX (**C**). MFI of the dyes in CD8$^+$CD44$^+$ T cells was measured by FACS analyses. (**D**) WT and *PTPMT1* KO CD8$^+$ T cells activated with CD3/CD28 antibodies were processed for γ-H2AX immunostaining followed by FACS analyses in the gated CD8$^+$CD44$^+$ effector T cells. Ultraviolet (UV) light–treated cells were used as the positive control, and isotype staining was used as the negative control. (**E**) Activated CD8$^+$ T cells were processed for apoptosis analyses. Annexin V$^+$ apoptotic cells in the CD8$^+$CD44$^+$ population were quantified by FACS analyses. 7-AAD, 7-aminoactinomycin D. (**F**) Bcl-2 levels in CD8$^+$CD44$^+$ effector T cell population were determined by FACS analyses. (**G** and **H**) *PTPMT1* KO CD8$^+$ T cells were activated with CD3/CD28 antibodies in the presence of the AMPK inhibitor dorsomorphin (300 nM) or vehicle control. Cells were then washed with XF base medium and resuspended in XF base medium without metabolic substrates. OCRs were measured following the injections of sodium pyruvate (5 mM), oligomycin (1.5 μM), FCCP (1.2 μM), and rotenone (1.0 μM) (G). Cells were also analyzed for ROS levels as described above (H). (**I** to **L**) CD8$^+$ T cells isolated from *PTPMT1* KO mice were activated with CD3/CD28 antibodies in the presence of NAC at the indicated concentrations. The cells were harvested and analyzed for apoptosis, cell division, IFN-γ, and granzyme B by FACS analyses. Data are presented as means ± SD of biological replicates. **P* < 0.05, ***P* < 0.01, and ****P* < 0.001.

pyruvate utilization was responsible for the functional defects of *PTPMT1* KO CD8$^+$ T cells, we generated T cell–specific *MPC2* KO mice (*MPC2*$^{fl/fl}$/*Lck-Cre*$^+$). Upon T cell receptor stimulation, CD25$^+$ and CD69$^+$ early activated CD8$^+$ T cells displayed no changes between *MPC2* KO and WT groups (Fig. 9, A to C). However, IFN-γ$^+$–producing and granzyme B$^+$ effector cells (Fig. 9, A, D, and E) and cell division (Fig. 9, A, and F) were significantly decreased in *MPC2* KO cells. Furthermore, the levels of ROS (Fig. 9G) and apoptosis (Fig. 9H) were increased in the KO cells, resembling the phenotypes observed in *PTPMT1* KO cells. Consistent with these data, treatment of WT CD8$^+$ T cells with UK5099, a well-established potent MPC inhibitor (*47*), showed a minimal effect on the activation of naïve CD8$^+$ T cells (Fig. 9, I and J) but decreased effector cell production (Fig. 9, K

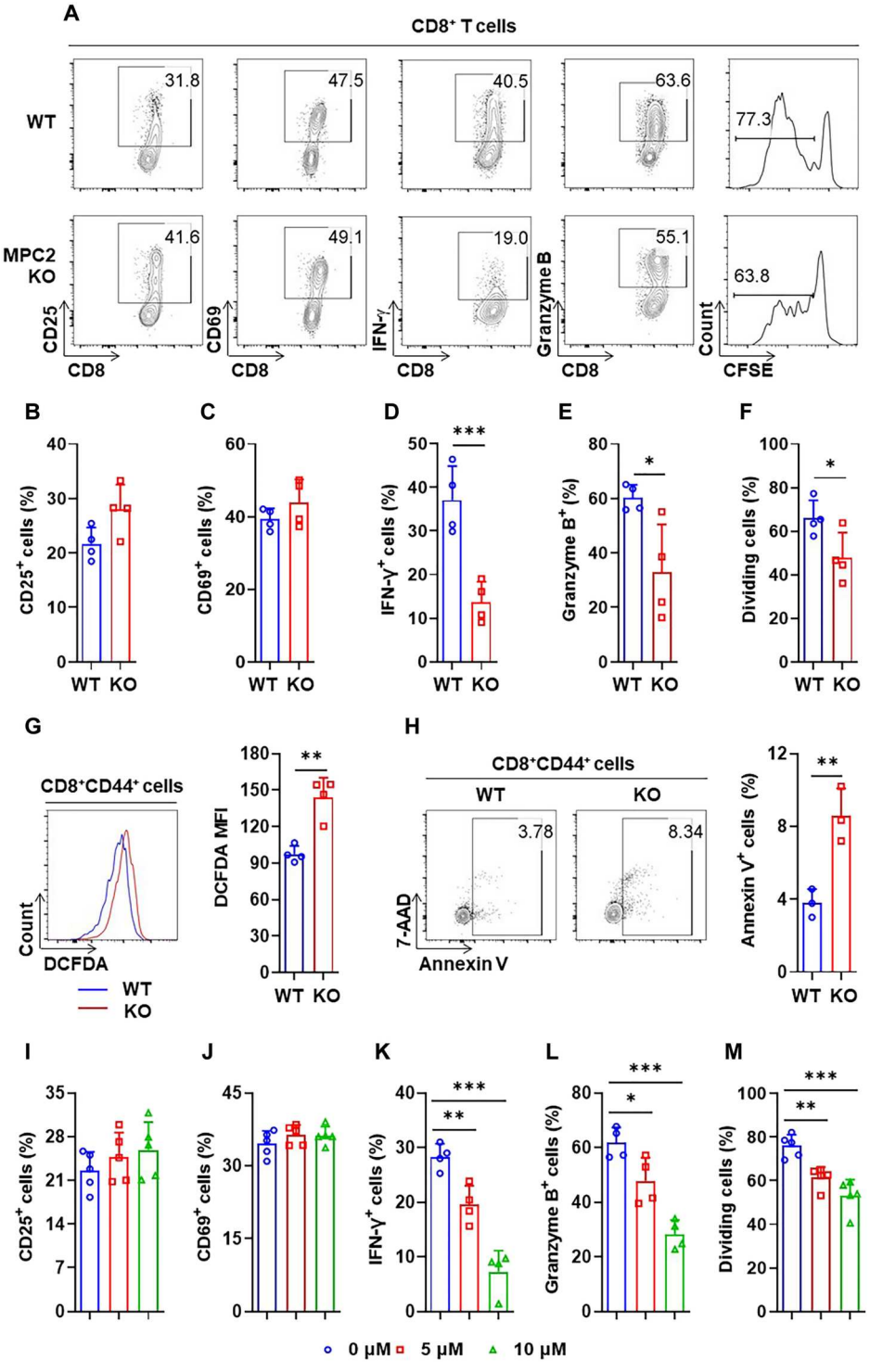

Fig. 9. Mitochondrial oxidation of pyruvate is essential for CD8⁺ effector T cell development. (**A** to **F**) *MPC2*$^{fl/fl}$/*Lck-Cre*$^{+}$ (*MPC2* KO) mice were generated, and CD8^{+} T cells isolated from *MPC2* KO and WT (*MPC2*$^{+/+}$/*Lck-Cre*$^{+}$) control mice were activated by CD3/CD28 antibodies. Early activation markers CD25 and CD69 were examined at day 1 [(A) to (C)]. IFN-γ–expressing and granzyme B^{+} effector cells were determined by FACS analyses at day 3 (A to E). Cell division was examined by the CFSE dilution assay on day 3 [(A) to (F)]. (**G** and **H**) Activated CD8^{+} T cells were processed for ROS and apoptosis analyses. MFI of DCFDA (G) and annexin V^{+} apoptotic cells (H) in the CD8^{+}CD44^{+} effector cell population were quantified by FACS analyses. (**I** to **M**) CD8^{+} T cells isolated from WT C57BL/6 mice were activated by CD3/CD28 antibodies in the presence of UK5099 at the indicated concentrations. Cells were examined for early activation markers CD25 and CD69 at day 1 [(I) and (J)]. IFN-γ–expressing and granzyme B^{+} effector cells were determined by FACS at day 3 [(K) and (L)]. Cell division was examined by the CFSE dilution assay on day 3 (M). Data are presented as means ± SD of biological replicates. *P < 0.05, **P < 0.01, and ***P < 0.001.

and L) and cell division (Fig. 9M) in a dose-dependent manner, verifying the important role of mitochondrial oxidation of pyruvate in $CD8^+$ effector cell development. The fact that the genetic deletion or pharmacological blockade of the MPC recapitulated the effect of *PTPMT1* KO on $CD8^+$ effector cell development suggests that the $CD8^+$ T cell functional defects caused by *PTPMT1* deletion were mediated largely by diminished mitochondrial pyruvate uptake.

DISCUSSION

Mitochondria use competing substrates to produce energy and metabolites for macromolecule synthesis or epigenetic regulation of cell fate and function. Cytotoxic $CD8^+$ T cells play an essential role in adaptive immune responses. Our data in this report suggest that mitochondria in $CD8^+$ T cells must stay flexible in selecting substrates for energy production and intermediatory metabolism. This metabolic flexibility is essential for effector cell development, stem-like $CD8^+$ T cell maintenance, and the prevention of $CD8^+$ T cell exhaustion. Skewed substrate utilization from carbohydrates (via pyruvate) toward fatty acids and glutamate such as that caused by the depletion of the mitochondria-based phosphatase *PTPMT1* results in mitochondrial metabolic inflexibility, leading to diminished antitumor immunity.

$CD8^+$ T cells have different functional states during the life cycle, and they experience dynamic changes in energy sources and oxygen levels in various microenvironments. Within the tumor microenvironment, $CD8^+$ T cells exhibit high heterogeneity, including exhausted T cells and tumor antigen–specific memory/stem-like T cells (*48*). Because of their diverse functional states, they have distinct metabolic requirements (*7*–*9*). We find that PTPMT1-mediated mitochondrial metabolism from carbohydrates plays a crucial role in the expansion of $CD8^+$ effector cells, although effector T cells exploit primarily aerobic glycolysis for energy production (*7*–*9*). This is evidenced by reduced populations of IFN-γ–producing and granzyme B^+ cells in both in vitro activated $CD8^+$ T cells and in vivo $CD8^+$ T cells isolated from tumors and TDLNs. PTPMT1 is also important for the specification and maintenance of subsequent subpopulations derived from effector cells. *PTPMT1* depletion from naïve $CD8^+$ T cells significantly increased the population of exhausted $CD8^+$ T cells and decreased that of stem-like $CD8^+$ T cells in both the tumor microenvironment and TDLNs. Furthermore, depleting *PTPMT1* after the expansion of $CD8^+$ effector T cells in tumor-bearing mice produced similar phenotypes in these $CD8^+$ subpopulations. These results suggest that persistently skewed/forced mitochondrial utilization toward fatty acids and glutamate is detrimental to stem-like $CD8^+$ T cell development and/or maintenance, although $CD8^+$ memory T cells prefer to use fatty acids for oxidative phosphorylation (*7*–*9*).

Persistent mitochondrial substrate shift and the inability to adapt fuel oxidation to fuel availability can cause mitochondrial overload/congestion, gridlock, and damage (*49*). Indeed, biased mitochondrial substrate utilization of fatty acids/glutamate and metabolic inflexibility resulted in oxidative stress in *PTPMT1* KO $CD8^+$ T cells. Cellular ROS and mitochondrial superoxide levels were doubled in these KO cells. The oxidative stress, in turn, induced DNA damage, cell cycle delay, and apoptosis since the treatment with the antioxidant NAC completely reversed cell death and largely rescued effector cell development in *PTPMT1* KO $CD8^+$ T cells. Nonetheless, targeted deletion of *PTPMT1* specifically in established exhausted and stem-like $CD8^+$ T cells in the tumor microenvironment would offer better models for investigating the precise role of PTPMT1-mediated oxidation of carbohydrates in these distinct cell populations and their impact on antitumor immunity.

Another important finding in this report is that PTPMT1 plays an important role in governing the metabolic fate of pyruvate, maintaining mitochondrial metabolic plasticity. *PTPMT1* depletion caused minimal defects in the mitochondrial machinery. Mitochondrial content was normal, and the electron transport chain worked fine in *PTPMT1* KO cells since succinate-supported mitochondrial respiration was similar in PTPMT1 null and WT mitochondria. Moreover, steady-state total cellular ATP levels were maintained in *PTPMT1* KO cells with full access to all substrates. However, the loss of PTPMT1 resulted in biased substrate selection in mitochondria. The utilization of pyruvate, a key mitochondrial substrate derived from glucose (a simple carbohydrate), was inhibited, whereas fatty acid and glutamate utilizations were enhanced.

Pyruvate is a key metabolite derived from glucose. It is at the central branch point of mitochondrial oxidation and cytosolic glycolysis in glucose metabolism—it can enter the mitochondrion for oxidation or be reduced to lactate in the cytosol. PTPMT1 appears to facilitate mitochondrial utilization of pyruvate since ATP synthesis–driven oxygen consumption of PTPMT1-ablated mitochondria was greatly reduced when pyruvate was used as the sole substrate. This notion is verified by pyruvate uptake analyses in which PTPMT1 null mitochondria showed >80% reduction in up-taking pyruvate compared to WT control mitochondria. The observation that the TCA cycle was disrupted while total cellular pyruvate levels were increased in *PTPMT1* deleted cells provides additional support. These data also suggest that the suppression of mitochondrial selection for pyruvate was most likely responsible for the remodeled metabolism in *PTPMT1* KO cells. Furthermore, the fact that *PTPMT1* deletion recapitulated the phenotypes demonstrated by mitochondrial pyruvate transporter (*MPC2*) KO $CD8^+$ T cells also strongly supports that the functional defects of *PTPMT1* KO cells were largely caused by the inhibition of pyruvate oxidation.

The precise mechanism by which PTPMT1 facilitates mitochondrial utilization/uptake of pyruvate remains to be further determined. PTPMT1 is localized to the mitochondrial inner membrane where pyruvate transporters reside. This phosphatase dephosphorylates PIPs phosphatidylinositol 3,5-bisphosphate [PI(3,5)P_2] and phosphatidylinositol 5-phosphate (PI5P) (*17*, *18*). PIPs serve as second messengers by binding to effector proteins, including ion channels and transporters (*50*, *51*). We have shown previously that PI(3,5)P_2 and PI5P directly promote fatty acid–induced activation of UCP2 (*20*), a C4 metabolite transporter (*21*) that inhibits mitochondrial oxidation of glucose but enhances cytosolic glycolysis (*22*–*25*). Conceivably, *PTPMT1* depletion leads to the buildup of downstream PIP substrates in the inner membrane, which, in turn, remodel mitochondrial energy source selection by enhancing UCP2. Nevertheless, it remains to be determined whether PIPs can directly interact with the pyruvate transporter MPC and regulate its activity. In addition, PTPMT1 has been shown to be involved in the synthesis of cardiolipin (*19*), which is one of the major components of the mitochondrial inner membrane and is important for maintaining mitochondrial membrane stability and dynamics. Impaired cardiolipin production affects $CD8^+$ effector cell function, and cardiolipin-deficient $CD8^+$ T

cells fail to respond to pathogens (*52*). It may be possible that *PTPMT1* depletion decreases mitochondrial pyruvate utilization also partly through the reduction in cardiolipin synthesis.

In summary, we demonstrate in this report that the mitochondrial phosphatase PTPMT1 plays an essential role in facilitating mitochondrial utilization of carbohydrates and maintaining mitochondrial metabolic flexibility, which is critically important for $CD8^+$ T cells to rapidly adapt to environmental metabolic cues and cell-intrinsic energetic/biosynthetic demands. Disruption of mitochondrial substrate selection flexibility and prolonged biased utilization of fatty acids/glutamate as seen in *PTPMT1* KO cells impair $CD8^+$ effector cell development and stem-like $CD8^+$ T cell maintenance, and accelerate $CD8^+$ T cell exhaustion. These findings hold an important implication—it is advised to avoid using pharmacological interventions that target cancer cell metabolism by inhibiting their carbohydrate utilization during cancer immunotherapy. These interventions can inadvertently hinder $CD8^+$ T cell antitumor responses and compromise the therapeutic effectiveness of cancer immunotherapy.

MATERIALS AND METHODS

Mice

PTPMT1$^{fl/+}$ mice were generated in our previous study (*20*). *MPC2*$^{fl/+}$ (strain no. 032118) (*43*), *Lck-Cre*$^+$ (strain no. 003802) (*53*), *Mx1-Cre*$^+$ (strain no. 003556) (*29*), B6 Thy1.1$^+$ (strain no. 000406), C57BL/6 (CD45.2$^+$) (strain no. 000664), and congenic BoyJ (CD45.1$^+$) mice (strain no. 002014) were purchased from the Jackson laboratory. OT-I transgenic mice (model no. 2334) (*54*) were obtained from Taconic Biosciences. All mice were kept under specific pathogen–free conditions at Emory University Division of Animal Resources. Animal procedures complied with the National Institutes of Health Guidelines for the Care and Use of Laboratory Animals and were approved by the Institutional Animal Care and Use Committee (PROTO no. 201700884).

T cell activation and division assays

$CD8^+$ T cells were isolated from spleens and lymph nodes by negative selection with magnetic cell sorting columns (Miltenyi Biotec) following the manufacturer's protocol. Purified $CD8^+$ T cells were stimulated with mouse T-activator CD3/CD28 antibody–coupled Dynabeads (Thermo Fisher Scientific). The cells were examined for the activation status by fluorescence-activated cell sorting (FACS) analyses for the markers CD25 and CD69 24 hours after stimulation. The effector cell differentiation was determined on the basis of FACS analyses for IFN-γ–producing and granzyme B^+ cells 72 hours after stimulation. To activate OT-I $CD8^+$ T cells, $CD8^+$ T cells isolated from the spleen and lymph nodes dissected from OT-I mice were stimulated with the peptide SIINFEKL (OVA257-264) (1 μM; Sigma-Aldrich) for 24 hours and then expanded for additional 4 days. All $CD8^+$ T cells were cultured in T cell medium [RPMI 1640 medium supplemented with fetal bovine serum (10%; Gibco), GlutaMAX (1%; Gibco), penicillin-streptomycin (1%; Hyclone), sodium pyruvate (1%; Hyclone), nonessential amino acids (1%; Hyclone), β-mercaptoethanol (50 μM), and recombinant human interleukin-2 (50 U/ml; PeproTech).

T cell division was measured by the CFSE dilution assay. $CD8^+$ T cells were incubated with CFSE (5 μM) at 37°C for 15 min and then washed three times with medium. CFSE-labeled cells were activated with CD3/CD28 antibody–coupled Dynabeads as described above. Cell division was measured by FACS analyses for $CFSE^+$ cells 72 hours later.

Isolation of lymphocytes from tumors and TDLNs

To isolate tumor-infiltrating lymphocytes (TILs), tumor tissues were mechanically minced and treated with collagenase type IV (1 mg/ml; Thermo Fisher Scientific) at 37°C for 20 min. The mixture was then thoroughly triturated and passed through 70-μm filters. TILs were subsequently enriched by density gradient centrifugation using lymphocyte separation medium (Corning Inc.). For isolation of lymphocytes from TDLNs, axillary and inguinal lymph nodes dissected from tumor-bearing mice were processed for generation of single-cell suspensions, as described above.

FACS analysis

FACS analyses were performed on a Cytoflex flow cytometer (Beckman Coulter Life Sciences), as previously described (*20*, *55*). Briefly, single-cell suspensions were surface stained with surface markers antibodies labeled with various fluorochromes (eBiosciences Inc., BioLegend, and BD Biosciences). Dead cells were excluded on the basis of 4′,6-diamidino-2-phenylindole staining. For intracellular cytokine staining, cells were stimulated with phorbol-12-myristate 13-acetate (80 nM) and ionomycin (1.4 μM) (BioLegend) in the presence of the endoplasmic reticulum–Golgi protein trafficking inhibitor brefeldin A (5 μg/ml) at 37°C for 4 hours. After being stained for surface antigens, cells were fixed and permeabilized using a Cytofix/Cytoperm kit (BD Biosciences) following the manufacturer's instructions. For intracellular detection of Tcf1, Bcl-2, PTPMT1, and γ-H2AX, surface-stained cells were fixed with 4% formaldehyde and then permeabilized using the BD Pharmingen transcription factor buffer set (BD Biosciences), followed by intracellular staining. For cell cycle analyses, activated $CD8^+$ T cells were stained with cell surface markers, fixed, permeabilized using a Cytofix/Cytoperm kit, stained with Ki-67 antibody (BioLegend), and further incubated with Hoechst 33342 (20 mg/ml). The cells were then analyzed by FACS.

To measure cellular ROS levels, cells were incubated in phosphate-buffered saline (PBS) containing DCFDA (5 μM) (Thermo Fisher Scientific) at 37°C for 15 min and then washed with PBS. ROS levels were quantified by FACS analyses. Determinations of mitochondrial mass and mitochondrial superoxide were performed with MitoTracker Green (100 nM; Thermo Fisher Scientific) and MitoSOX Red (5 μM; Thermo Fisher Scientific), respectively. These dyes were added to cultured cells and incubated at 37°C for 15 min. Cells were washed with PBS and then processed for cell surface markers staining. To detect neutral lipid droplets, cells were incubated with BODIPY 493/503 (4,4-difluoro-1,3,5,7,8-pentamethyl-4-bora-3a,4a-diaza-*s*-indacene) (2 μM; Thermo Fisher Scientific) at 37°C for 15 min, washed with PBS, and then analyzed by FACS. For apoptosis analyses, cells were stained for cell surface antigens and then incubated with annexin V (2.5 μg/ml) and 7-aminoactinomycin D (5 μg/ml; BD Biosciences). Apoptotic cells (annexin V^+) were quantified by FACS analyses. Data analyses were performed using FlowJo software (Tree Star).

Transmigration assay

Transmigration assays were carried out with 8.0-μm pore transwells (Corning). Activated WT and *PTPMT1* KO $CD8^+$ T cells were

washed with RPMI 1640 medium twice, resuspended in RPMI 1640 medium containing fatty acid–free bovine serum albumin (BSA) (0.1%). WT cells (2.5×10^5) were labeled with CFSE (1.0 μM) and mixed with *PTPMT1* KO $CD8^+$ T cells (2.5×10^5) in 100 μl of medium and loaded into the upper chamber. Six hundred microliters of RPMI 1640 medium supplemented with fatty acid–free BSA (0.1%) and S1P (100 nM) (Tocris) was added to the lower chamber. After incubation at 37°C for 90 min, input cells, cells collected from the upper chamber, and cells collected from the lower chambers were analyzed by FACS. Migration efficiency was then calculated.

LCMV infection

LCMV (strain Armstrong) was propagated, titered, and used as previously described (*56*). Mice were infected with 2×10^5 plaque-forming units of LCMV intraperitoneally to initiate acute infection and euthanized at day 8 after infection for FACS analyses of $CD8^+$ T cells. For detecting LCMV-specific $CD8^+$ T cell responses, LCMV gp33 and gp276-specific tetramers were prepared as described previously (*57*).

Measurement of oxygen consumption in living cells

Measurement of respiration of living T cells with full access to all metabolic substrates was performed using a Seahorse XF24 metabolic flux analyzer (Agilent) as previously described (*20*). Briefly, activated $CD8^+$ T cells (5×10^5 cells) were seeded in Cell-Tak precoated XF24 cell culture mini plates and incubated in XF base medium with glucose (10 mM), L-glutamine (2 mM), and sodium pyruvate (1 mM) at 37°C for 1 hour. OCRs were measured at the basal level and following the addition of mitochondrial inhibitor oligomycin (1.5 μM), mitochondrial-uncoupling compound FCCP (1.2 μM), and respiratory chain inhibitor rotenone (1 μM). Glycolytic activities were measured simultaneously using the same instrument based on the ECARs. To determine whether the hyperactivation of AMPK affects pyruvate utilization, *PTPMT1* KO $CD8^+$ T cells were activated by CD3/CD28 antibodies for 72 hours in the presence or absence of the AMPK inhibitor dorsomorphin (300 nM) (MilliporeSigma), washed with XF base medium, and then resuspended in XF base medium without metabolic substrates. OCRs were measured following the injections of pyruvate (5 mM), oligomycin (1.5 μM), FCCP (1.2 μM), and rotenone (1.0 μM). All measurements were performed following the manufacturer's instructions and protocols. Data were normalized against cell numbers.

Measurement of respiration in isolated mitochondria

Respiration of mitochondria was measured on a Seahorse XF24 metabolic flux analyzer as previously described (*58*). Briefly, mitochondria (10 μg of protein) freshly isolated from the liver were plated in an XF24 plate in 50 μl of 1× mitochondrial assay solution [pH 7.4; sucrose (70 mM), mannitol (220 mM), KH_2PO_4 (5 mM), $MgCl_2$ (5 mM), Hepes (2 mM), EGTA (1 mM), and fatty acid–free BSA (0.2%)]. XF24 plates were centrifuged at 2000*g* at 4°C for 20 min, and then 450 μl of mitochondrial assay solution containing pyruvate (5 mM)/malate (5 mM), glutamate (5 mM)/malate (5 mM), palmitoyl-CoA (40 μM)/carnitine (40 μM)/malate (5 mM), or succinate (10 mM) was added to each well. Plates were incubated at 37°C in a non-CO2 incubator for 10 min. OCRs were measured under basal conditions in the presence of adenosine 5′-diphosphate (ADP; 4 mM), oligomycin (1.5 μM), FCCP (4 μM), and rotenone (1 μM), as described above.

Pyruvate uptake assay

The pyruvate uptake assay was performed following a previously published methodology (*59*). Aliquots of mitochondria were diluted in 100 μl of uptake buffer [120 mM KCL, 5 mM KH_2PO_4, 1 mM EGTA, 5 mM Hepes (pH 7.4), 2 μM rotenone, and 2 μM antimycin A]. One hundred microliters of mitochondria suspension were rapidly mixed with 100 μl of 2× pyruvate buffer (uptake buffer, pH 6.1 mixed with 5 mM ^{13}C-pyruvate at the 1:1 ratio) generating the pH gradient needed to initiate uptake. Three minutes later, 200 μl of stop buffer [uptake buffer, pH 6.8 mixed with 10 mM α-cyano-4-hydroxycinnamic acid (CHC) at the ratio of 9:1] was rapidly mixed with the samples to halt uptake. Mitochondria were washed three times with 1000 μl of wash buffer [uptake buffer, pH 6.8 supplemented with CHC (2 mM) and pyruvate (10 mM)] and then lysed. Levels of ^{13}C-pyruvate in the lysates were quantified using liquid chromatography–tandem mass spectrometry.

RNA-seq analyses

Purified $CD8^+$ T cells were activated by CD3/CD28 antibody–coupled Dynabeads for 72 hours. Total RNA was isolated with a Monarch total RNA miniprep kit (New England Biolabs). RNA-seq libraries were prepared by TruSeq stranded mRNA sample preparation kit (Illumina) and sequenced as 75–base pair paired-end reads with HiSeq2500 (Illumina) (three biological replicates per group). Reference genome and gene model annotation files were downloaded from https://genome.ucsc.edu. The index of the reference genome was built using Hisat2 v2.0.5, and paired-end clean reads were aligned to the reference genome using Hisat2 v2.0.5. FeatureCounts v1.5.0-p3 was used to count read numbers mapped to each gene. Fragments per kilobase of feature per million mapped reads (FPKM) of each gene was then calculated on the basis of the length of the gene and the reads count mapped to this gene. Differential expression genes were identified as those with fold changes of >2 and a false discovery rate of <0.05 using DESeq2 (*60*). Enrichment analyses were performed using KEGG (Kyoto Encyclopedia of Genes and Genomes). ClusterProfiler R package was used to test the statistical enrichment of differential expression genes in KEGG pathways. The raw sequence reads from RNA-seq experiments have been deposited in the National Center for Biotechnology Information (NCBI) Gene Expression Omnibus database (https://ncbi.nlm.nih.gov/geo/) and are accessible with the accession no. GSE216523.

Metabolomic analysis

Purified $CD8^+$ T cells were activated by CD3/CD28 antibody–coupled Dynabeads for 72 hours and then harvested for metabolomic analyses. Briefly, cells were washed in PBS and mixed with 800 μl of methanol containing internal standards (10 μM; Human Metabolomics Technologies). Five hundred fifty microliters of Milli-Q water were added and mixed thoroughly. Extracts were centrifuged (2300*g* at 4°C for 5 min), and supernatants (350 μl) were filtrated through 5-kDa cutoff filters (ULTRAFREE-MC-PLHCC, Human Metabolome Technologies) to remove macromolecules. Filtrates were centrifugally concentrated and resuspended in 25 μl of ultrapure water immediately before the measurements. Targeted

quantitative analyses were performed using capillary electrophoresis mass spectrometry (capillary electrophoresis time-of-flight mass spectrometry and capillary electrophoresis-triple quadrupole mass spectrometry) in the cation and anion analysis modes for analyzing cationic and anionic metabolites, respectively.

Statistics and reproducibility

Unless otherwise noted, data are presented as means ± SD of biological replicates (independent animals/independent experiments) (n numbers are shown on graphics or specified in figure legends). Unpaired two-tailed Student's t test was used for the statistical comparison of the two groups. $^{*}P < 0.05$; $^{**}P < 0.01$; $^{***}P < 0.001$.

Supplementary Materials

This PDF file includes:

Figs. S1 to S8

REFERENCES AND NOTES

1. B. H. Goodpaster, L. M. Sparks, Metabolic flexibility in health and disease. *Cell Metab.* **25**, 1027–1036 (2017).
2. M. Hashimoto, A. O. Kamphorst, S. J. Im, H. T. Kissick, R. N. Pillai, S. S. Ramalingam, K. Araki, R. Ahmed, CD8 T cell exhaustion in chronic infection and cancer: Opportunities for interventions. *Annu. Rev. Med.* **69**, 301–318 (2018).
3. S. J. Im, M. Hashimoto, M. Y. Gerner, J. Lee, H. T. Kissick, M. C. Burger, Q. Shan, J. S. Hale, J. Lee, T. H. Nasti, A. H. Sharpe, G. J. Freeman, R. N. Germain, H. I. Nakaya, H. H. Xue, R. Ahmed, Defining $CD8^+$ T cells that provide the proliferative burst after PD-1 therapy. *Nature* **537**, 417–421 (2016).
4. C. S. Eberhardt, H. T. Kissick, M. R. Patel, M. A. Cardenas, N. Prokhnevska, R. C. Obeng, T. H. Nasti, C. C. Griffith, S. J. Im, X. Wang, D. M. Shin, M. Carrington, Z. G. Chen, J. Sidney, A. Sette, N. F. Saba, A. Wieland, R. Ahmed, Functional HPV-specific $PD\text{-}1^+$ stem-like CD8 T cells in head and neck cancer. *Nature* **597**, 279–284 (2021).
5. D. T. Utzschneider, M. Charmoy, V. Chennupati, L. Pousse, D. P. Ferreira, S. Calderon-Copete, M. Danilo, F. Alfei, M. Hofmann, D. Wieland, S. Pradervand, R. Thimme, D. Zehn, W. Held, T cell factor 1-expressing memory-like $CD8^+$ T cells sustain the immune response to chronic viral infections. *Immunity* **45**, 415–427 (2016).
6. R. He, S. Hou, C. Liu, A. Zhang, Q. Bai, M. Han, Y. Yang, G. Wei, T. Shen, X. Yang, L. Xu, X. Chen, Y. Hao, P. Wang, C. Zhu, J. Ou, H. Liang, T. Ni, X. Zhang, X. Zhou, K. Deng, Y. Chen, Y. Luo, J. Xu, H. Qi, Y. Wu, L. Ye, Follicular CXCR5- expressing $CD8^+$ T cells curtail chronic viral infection. *Nature* **537**, 412–428 (2016).
7. R. I. K. Geltink, R. L. Kyle, E. L. Pearce, Unraveling the complex interplay between T cell metabolism and function. *Annu. Rev. Immunol.* **36**, 461–488 (2018).
8. J. T. Chang, E. J. Wherry, A. W. Goldrath, Molecular regulation of effector and memory T cell differentiation. *Nat. Immunol.* **15**, 1104–1115 (2014).
9. M. D. Buck, R. T. Sowell, S. M. Kaech, E. L. Pearce, Metabolic instruction of immunity. *Cell* **169**, 570–586 (2017).
10. C. H. Chang, J. D. Curtis, L. B. Maggi Jr., B. Faubert, A. V. Villarino, D. O'Sullivan, S. C. C. Huang, G. J. W. van der Windt, J. Blagih, J. Qiu, J. D. Weber, E. J. Pearce, R. G. Jones, E. L. Pearce, Posttranscriptional control of T cell effector function by aerobic glycolysis. *Cell* **153**, 1239–1251 (2013).
11. N. M. Chapman, M. R. Boothby, H. Chi, Metabolic coordination of T cell quiescence and activation. *Nat. Rev. Immunol.* **20**, 55–70 (2020).
12. E. M. Steinert, K. Vasan, N. S. Chandel, Mitochondrial metabolism regulation of T cell-mediated immunity. *Annu. Rev. Immunol.* **39**, 395–416 (2021).
13. T. N. Tarasenko, S. E. Pacheco, M. K. Koenig, J. Gomez-Rodriguez, S. M. Kapnick, F. Diaz, P. M. Zerfas, E. Barca, J. Sudderth, R. J. DeBerardinis, R. Covian, R. S. Balaban, S. DiMauro, P. J. McGuire, Cytochrome c oxidase activity is a metabolic checkpoint that regulates cell fate decisions during T cell activation and differentiation. *Cell Metab.* **25**, 1254–1268. e7 (2017).
14. L. A. Sena, S. Li, A. Jairaman, M. Prakriya, T. Ezponda, D. A. Hildeman, C. R. Wang, P. T. Schumacker, J. D. Licht, H. Perlman, P. J. Bryce, N. S. Chandel, Mitochondria are required for antigen-specific T cell activation through reactive oxygen species signaling. *Immunity* **38**, 225–236 (2013).
15. S. A. Vardhana, M. A. Hwee, M. Berisa, D. K. Wells, K. E. Yost, B. King, M. Smith, P. S. Herrera, H. Y. Chang, A. T. Satpathy, M. R. M. van den Brink, J. R. Cross, C. B. Thompson, Impaired mitochondrial oxidative phosphorylation limits the self-renewal of T cells exposed to persistent antigen. *Nat. Immunol.* **21**, 1022–1033 (2020).
16. D. J. Pagliarini, S. E. Wiley, M. E. Kimple, J. R. Dixon, P. Kelly, C. A. Worby, P. J. Casey, J. E. Dixon, Involvement of a mitochondrial phosphatase in the regulation of ATP production and insulin secretion in pancreatic beta cells. *Mol. Cell* **19**, 197–207 (2005).
17. D. J. Pagliarini, C. A. Worby, J. E. Dixon, A PTEN-like phosphatase with a novel substrate specificity. *J. Biol. Chem.* **279**, 38590–38596 (2004).
18. J. Shen, X. Liu, W. M. Yu, J. Liu, M. Groot Nibbelink, C. Guo, T. Finkel, C. K. Qu, A critical role of mitochondrial phosphatase Ptpmt1 in embryogenesis reveals a mitochondrial metabolic stress-induced differentiation checkpoint in embryonic stem cells. *Mol. Cell. Biol.* **31**, 4902–4916 (2011).
19. J. Zhang, Z. Guan, A. N. Murphy, S. E. Wiley, G. A. Perkins, C. A. Worby, J. L. Engel, P. Heacock, O. K. Nguyen, J. H. Wang, C. R. H. Raetz, W. Dowhan, J. E. Dixon, Mitochondrial phosphatase PTPMT1 is essential for cardiolipin biosynthesis. *Cell Metab.* **13**, 690–700 (2011).
20. W. M. Yu, X. Liu, J. Shen, O. Jovanovic, E. E. Pohl, S. L. Gerson, T. Finkel, H. E. Broxmeyer, C. K. Qu, Metabolic regulation by the mitochondrial phosphatase PTPMT1 is required for hematopoietic stem cell differentiation. *Cell Stem Cell* **12**, 62–74 (2013).
21. A. Vozza, G. Parisi, F. de Leonardis, F. M. Lasorsa, A. Castegna, D. Amorese, R. Marmo, V. M. Calcagnile, L. Palmieri, D. Ricquier, E. Paradies, P. Scarcia, F. Palmieri, F. Bouillaud, G. Fiermonte, UCP2 transports C4 metabolites out of mitochondria, regulating glucose and glutamine oxidation. *Proc. Natl. Acad. Sci. U.S.A.* **111**, 960–965 (2014).
22. F. Bouillaud, UCP2, not a physiologically relevant uncoupler but a glucose sparing switch impacting ROS production and glucose sensing. *Biochim. Biophys. Acta* **1787**, 377–383 (2009).
23. S. Diano, T. L. Horvath, Mitochondrial uncoupling protein 2 (UCP2) in glucose and lipid metabolism. *Trends Mol. Med.* **18**, 52–58 (2012).
24. C. Pecqueur, T. Bui, C. Gelly, J. Hauchard, C. Barbot, F. Bouillaud, D. Ricquier, B. Miroux, C. B. Thompson, Uncoupling protein-2 controls proliferation by promoting fatty acid oxidation and limiting glycolysis-derived pyruvate utilization. *FASEB J.* **22**, 9–18 (2008).
25. I. Samudio, M. Fiegl, M. Andreeff, Mitochondrial uncoupling and the Warburg effect: Molecular basis for the reprogramming of cancer cell metabolism. *Cancer Res.* **69**, 2163–2166 (2009).
26. F. O. Bagger, D. Sasivarevic, S. H. Sohi, L. G. Laursen, S. Pundhir, C. K. Sønderby, O. Winther, N. Rapin, B. T. Porse, BloodSpot: A database of gene expression profiles and transcriptional programs for healthy and malignant haematopoiesis. *Nucleic Acids Res.* **44**, D917–D924 (2016).
27. G. Monaco, B. Lee, W. Xu, S. Mustafah, Y. Y. Hwang, C. Carré, N. Burdin, L. Visan, M. Ceccarelli, M. Poidinger, A. Zippelius, J. Pedro de Magalhães, A. Larbi, RNA-seq signatures normalized by mRNA abundance allow absolute deconvolution of human immune cell types. *Cell Rep.* **26**, 1627–1640.e7 (2019).
28. D. Doughty-Shenton, J. D. Joseph, J. Zhang, D. J. Pagliarini, Y. Kim, D. Lu, J. E. Dixon, P. J. Casey, Pharmacological targeting of the mitochondrial phosphatase PTPMT1. *J. Pharmacol. Exp. Ther.* **333**, 584–592 (2010).
29. R. Kuhn, F. Schwenk, M. Aguet, K. Rajewsky, Inducible gene targeting in mice. *Science* **269**, 1427–1429 (1995).
30. G. Bocharov, J. Argilaguet, A. Meyerhans, Understanding experimental LCMV infection of mice: The role of mathematical models. *J. Immunol. Res.* **2015**, 739706 (2015).
31. M. J. Moore, N. E. Blachere, J. J. Fak, C. Y. Park, K. Sawicka, S. Parveen, I. Zucker-Scharff, B. Moltedo, A. Y. Rudensky, R. B. Darnell, ZFP36 RNA-binding proteins restrain T cell activation and anti-viral immunity. *eLife* **7**, (2018).
32. M. A. Ataide, K. Komander, K. Knöpper, A. E. Peters, H. Wu, S. Eickhoff, T. Gogishvili, J. Weber, A. Grafen, A. Kallies, N. Garbi, H. Einsele, M. Hudecek, G. Gasteiger, M. Hölzel, M. Vaeth, W. Kastenmüller, BATF3 programs $CD8^+$ T cell memory. *Nat. Immunol.* **21**, 1397–1407 (2020).
33. D. Mukherjee, L. S. Bercz, M. A. Torok, T. A. Mace, Regulation of cellular immunity by activating transcription factor 4. *Immunol. Lett.* **228**, 24–34 (2020).
34. J. Wittner, W. Schuh, Krüppel-like factor 2 (KLF2) in immune cell migration. *Vaccine* **9**, (2021).
35. G. Jeannet, C. Boudousquié, N. Gardiol, J. Kang, J. Huelsken, W. Held, Essential role of the Wnt pathway effector Tcf-1 for the establishment of functional CD8 T cell memory. *Proc. Natl. Acad. Sci. U.S.A.* **107**, 9777–9782 (2010).
36. S. Gautam, J. Fioravanti, W. Zhu, J. B. le Gall, P. Brohawn, N. E. Lacey, J. Hu, J. D. Hocker, N. V. Hawk, V. Kapoor, W. G. Telford, D. Gurusamy, Z. Yu, A. Bhandoola, H. H. Xue, R. Roychoudhuri, B. W. Higgs, N. P. Restifo, T. P. Bender, Y. Ji, L. Gattinoni, The transcription factor c-Myb regulates $CD8^+$ T cell stemness and antitumor immunity. *Nat. Immunol.* **20**, 337–349 (2019).
37. S. J. Im, B. T. Konieczny, W. H. Hudson, D. Masopust, R. Ahmed, PD-1+ stemlike CD8 T cells are resident in lymphoid tissues during persistent LCMV infection. *Proc. Natl. Acad. Sci. U.S.A.* **117**, 4292–4299 (2020).

38. M. Matloubian, C. G. Lo, G. Cinamon, M. J. Lesneski, Y. Xu, V. Brinkmann, M. L. Allende, R. L. Proia, J. G. Cyster, Lymphocyte egress from thymus and peripheral lymphoid organs is dependent on S1P receptor 1. *Nature* **427**, 355–360 (2004).
39. D. G. Hardie, AMP-activated protein kinase: An energy sensor that regulates all aspects of cell function. *Genes Dev.* **25**, 1895–1908 (2011).
40. B. Viollet, B. Guigas, J. Leclerc, S. Hébrard, L. Lantier, R. Mounier, F. Andreelli, M. Foretz, AMP-activated protein kinase in the regulation of hepatic energy metabolism: From physiology to therapeutic perspectives. *Acta Physiol* **196**, 81–98 (2009).
41. D. G. Hardie, AMPK: Positive and negative regulation, and its role in whole-body energy homeostasis. *Curr. Opin. Cell Biol.* **33**, 1–7 (2015).
42. J. Liang, G. B. Mills, AMPK: A contextual oncogene or tumor suppressor? *Cancer Res.* **73**, 2929–2935 (2013).
43. K. S. McCommis, Z. Chen, X. Fu, W. G. McDonald, J. R. Colca, R. F. Kletzien, S. C. Burgess, B. N. Finck, Loss of mitochondrial pyruvate carrier 2 in the liver leads to defects in gluconeogenesis and compensation via pyruvate-alanine cycling. *Cell Metab.* **22**, 682–694 (2015).
44. L. R. Gray, M. R. Sultana, A. J. Rauckhorst, L. Oonthonpan, S. C. Tompkins, A. Sharma, X. Fu, R. Miao, A. D. Pewa, K. S. Brown, E. E. Lane, A. Dohlman, D. Zepeda-Orozco, J. Xie, J. Rutter, A. W. Norris, J. E. Cox, S. C. Burgess, M. J. Potthoff, E. B. Taylor, Hepatic mitochondrial pyruvate carrier 1 is required for efficient regulation of gluconeogenesis and whole-body glucose homeostasis. *Cell Metab.* **22**, 669–681 (2015).
45. D. K. Bricker, E. B. Taylor, J. C. Schell, T. Orsak, A. Boutron, Y. C. Chen, J. E. Cox, C. M. Cardon, J. G. van Vranken, N. Dephoure, C. Redin, S. Boudina, S. P. Gygi, M. Brivet, C. S. Thummel, J. Rutter, A mitochondrial pyruvate carrier required for pyruvate uptake in yeast, Drosophila, and humans. *Science* **337**, 96–100 (2012).
46. S. Herzig, E. Raemy, S. Montessuit, J. L. Veuthey, N. Zamboni, B. Westermann, E. R. S. Kunji, J. C. Martinou, Identification and functional expression of the mitochondrial pyruvate carrier. *Science* **337**, 93–96 (2012).
47. J. C. Hildyard, C. Ammälä, I. D. Dukes, S. A. Thomson, A. P. Halestrap, Identification and characterisation of a new class of highly specific and potent inhibitors of the mitochondrial pyruvate carrier. *Biochim. Biophys. Acta* **1707**, 221–230 (2005).
48. Q. Huang, X. Wu, Z. Wang, X. Chen, L. Wang, Y. Lu, D. Xiong, Q. Liu, Y. Tian, H. Lin, J. Guo, S. Wen, W. Dong, X. Yang, Y. Yuan, Z. Yue, S. Lei, Q. Wu, L. Ran, L. Xie, Y. Wang, L. Gao, Q. Tian, X. Zhou, B. Sun, L. Xu, Z. Tang, L. Ye, The primordial differentiation of tumor-specific memory $CD8^+$ T cells as bona fide responders to PD-1/PD-L1 blockade in draining lymph nodes. *Cell* **185**, 4049–4066.e25 (2022).
49. D. M. Muoio, Metabolic inflexibility: When mitochondrial indecision leads to metabolic gridlock. *Cell* **159**, 1253–1262 (2014).
50. T. Balla, Phosphoinositide-derived messengers in endocrine signaling. *J. Endocrinol.* **188**, 135–153 (2006).
51. N. Gamper, M. S. Shapiro, Regulation of ion transport proteins by membrane phosphoinositides. *Nat. Rev. Neurosci.* **8**, 921–934 (2007).
52. M. Corrado, J. Edwards-Hicks, M. Villa, L. J. Flachsmann, D. E. Sanin, M. Jacobs, F. Baixauli, M. Stanczak, E. Anderson, M. Azuma, A. Quintana, J. D. Curtis, T. Clapes, K. M. Grzes, A. M. Kabat, R. Kyle, A. E. Patterson, R. K. Geltink, B. Amulic, C. G. Steward, D. Strathdee, E. Trompouki, D. O'Sullivan, E. J. Pearce, E. L. Pearce, Dynamic cardiolipin synthesis is required for $CD8^+$ T cell immunity. *Cell Metab.* **32**, 981–995.e7 (2020).
53. T. Hennet, F. K. Hagen, L. A. Tabak, J. D. Marth, T-cell-specific deletion of a polypeptide N-acetylgalactosaminyl-transferase gene by site-directed recombination. *Proc. Natl. Acad. Sci. U.S.A.* **92**, 12070–12074 (1995).
54. K. A. Hogquist, S. C. Jameson, W. R. Heath, J. L. Howard, M. J. Bevan, F. R. Carbone, T cell receptor antagonist peptides induce positive selection. *Cell* **76**, 17–27 (1994).
55. L. Dong, W. M. Yu, H. Zheng, M. L. Loh, S. T. Bunting, M. Pauly, G. Huang, M. Zhou, H. E. Broxmeyer, D. T. Scadden, C. K. Qu, Leukaemogenic effects of Ptpn11 activating mutations in the stem cell microenvironment. *Nature* **539**, 304–308 (2016).
56. E. J. Wherry, J. N. Blattman, K. Murali-Krishna, R. van der Most, R. Ahmed, Viral persistence alters CD8 T-cell immunodominance and tissue distribution and results in distinct stages of functional impairment. *J. Virol.* **77**, 4911–4927 (2003).
57. K. Murali-Krishna, J. D. Altman, M. Suresh, D. J. D. Sourdive, A. J. Zajac, J. D. Miller, J. Slansky, R. Ahmed, Counting antigen-specific CD8 T cells: A reevaluation of bystander activation during viral infection. *Immunity* **8**, 177–187 (1998).
58. H. Zheng, W. M. Yu, J. Shen, S. Kang, D. Hambardzumyan, J. Y. Li, Y. Shen, A. M. Kenney, J. Chen, C. K. Qu, Mitochondrial oxidation of the carbohydrate fuel is required for neural precursor/stem cell function and postnatal cerebellar development. *Sci. Adv.* **4**, eaat2681 (2018).
59. L. R. Gray, A. J. Rauckhorst, E. B. Taylor, A method for multiplexed measurement of mitochondrial pyruvate carrier activity. *J. Biol. Chem.* **291**, 7409–7417 (2016).
60. M. I. Love, W. Huber, S. Anders, Moderated estimation of fold change and dispersion for RNA-seq data with DESeq2. *Genome Biology* **15**2014). 10.1186/s13059-014-0550-8.

Acknowledgments: We are grateful for the technical support from Pediatrics/Winship Flow Cytometry shared resources. **Funding:** This work was supported by the National Institutes of Health grants HL162725, CA275964, and HL130995 (to C.-K.Q.) and a Winship Cancer Institute Invest$ Pilot Grant. **Author contributions:** C.C., H.Z., S.A., K.A., P.Z., and Z.L. conducted the research and summarized the data. E.M.H., M.L.F., and R.A. provided critical reagents and advice, discussed the work, and edited the manuscript. C.-K.Q. designed experiments and directed the entire study. C.C. and C.-K.Q. wrote the manuscript with input from the other authors. **Competing interests:** The authors declare that they have no competing interests. **Data and materials availability:** All data needed to evaluate the conclusions in the paper are present in the paper and/or the Supplementary Materials. The raw sequence reads from RNA-seq experiments have been deposited in the NCBI Gene Expression Omnibus (GEO) database (https://ncbi.nlm.nih.gov/geo/) with the accession no. GSE216523.

Submitted 22 November 2022
Accepted 7 November 2023
Published 6 December 2023
10.1126/sciadv.adf9522